State-Dependent Diffusion of a Harmonically Trapped Atom

Robert Fisher

A thesis submitted in partial fulfilment of the requirements for the degree of Master of Science in Physics.

The University of Auckland,
February 2006.

Abstract

We study the diffusion of a harmonically trapped atom. When a two-level atom is excited on or near resonance, spontaneous emission causes its amplitude of oscillation to fluctuate; the atom gradually heats up. We find that when the exciting field is a standing wave, the diffusion process can show surprising behaviour. Metastable states exist, where the spontaneous emission is almost completely turned off. These states correspond to amplitudes of oscillation where the time-averaged coupling strength is orders of magnitude smaller than that for a stationary atom. As it diffuses the atom spends most of its time oscillating at these 'metastable amplitudes'. At a qualitative level, an explanation is suggested by the motion of the atomic state on the Bloch sphere.

For a quantitative treatment, we analyze the problem in one dimension and for a classical driving field. A quantum trajectory description of the internal state of the atom is coupled to a classical treatment of the center-of-mass motion via momentum kicks at the times of the quantum jumps. First, results of numerical simulations are presented to demonstrate that metastable states exist. We then calculate the mean waiting time for spontaneous emission and see that it exhibits sharp resonances as a function of the amplitude of oscillation in the trap. These resonances locate the metastable amplitudes. An approximate analytic expression for the waiting time distribution is derived under the assumption that the mean waiting time is sufficiently large. The parameter dependence is explored, and efficient algorithms for numerical simulations are developed to thoroughly characterise the phenomenon.

Acknowledgements

I would like to acknowledge and thank the people who contributed to this thesis. My supervisor Howard Carmichael guided the project and provided many insights into the problems we encountered. He is also a skilled and patient teacher. My co-supervisor Matthew Collett offered clear explanations and valuable opinions whenever they were asked for. Levente Horvath was of great assistance throughout the project, especially with his collaboration on the numerical simulations that were performed. Over the past year I have had the pleasure of sharing my office with Andy Chia and Chang-Suk Noh, with whom I enjoyed many discussions about physics. They were also very helpful in the writing and formatting of my thesis. Finally I would like to thank my family for their support of my studies in physics.

Contents

Chapter 1

Introduction

The control and manipulation of single atoms is a fundamental physical problem. Progress in this area enables both the exploration of new regimes of physics and the development of new technologies. The subject has flourished over the past two decades as the laser has proven itself to be a successful tool in the cooling and trapping of atoms. The interaction of single atoms with the electromagnetic field has become an area where theory and experiment are closely linked.

The first single particle trapping experiments were performed using atomic ions [1]. In a common type of ion trap, the Paul trap, the ion is confined using a spatially inhomogeneous electromagnetic field oscillating at a radio frequency [2]. Applying the cooling schemes proposed by Hänsch and Schawlow [3], and Wineland and Dehmelt [4], it became possible to cool a single ion to the ground state of the trapping potential, confining it to a precise location [5]. The field of ion trapping has continued to develop, providing new insights into fundamental physics, new standards in precision time and frequency measurements, and a promising candidate for an elementary quantum information processor [6, 7]. Laser cooling and trapping of neutral atoms prospered after the development of the magneto-optical trap [8]. In this trap an external magnetic field produces Zeeman shifts of the magnetic sublevels of the atom, providing a spatially dependent force, while counterpropagating laser beams use the Doppler effect to cool the atoms by velocity dependent scattering. This development made temperatures of a few millikelvin easily accesible.

More recently, systems containing a single cold trapped atom have been implemented in the field of cavity quantum electrodynamics (cavity QED). These systems have application to quantum information science, particularly because of their potential to transmit quantum information over long distances [9]. Currently these systems employ a dipole trap to confine the atom, using lasers that are far off resonance with the atomic transition of interest [10]. These lasers produce a standing-wave so that the AC Stark effect provides the spatially varying potential required to trap the atom. A useful feature of the traps used in these experiments is that the potential is independent of the internal state of the atom; this means the atom remains trapped as it is driven near resonance by a cavity mode in the regime of strong coupling [11]. Furthermore, the position of the atom in the trap can be measured in real time [12].

The aim of this thesis is to investigate the atomic motion in systems such as these. We consider an atom oscillating back and forward in a trap potential while it is driven near

resonance by an electromagnetic field in a standing-wave configuration. The motion is not trivial since the atom gets kicked around as it absorbs and emits photons. There are several motives for studying a system such as this in detail:

- Measurements in certain systems containing trapped atoms driven by a standing-wave field can be expected to depend on the motion of the atom. This is because in a standing-wave the intensity of the driving field (and therefore the coupling strength) varies sinusoidally along the direction of propagation. The importance of transverse motion in cavity QED experiments where atomic beams are used (rather than trapped atoms) has been known for some time [13].
- Heating due to photon absorptions and emissions is a central problem in many systems containing cold trapped atoms, especially when the atom is driven near resonance.
- The system is of interest in its own right, as it provides an elementary example on which to study issues related to quantum measurement and the quantum-classical interface.

With these in mind we develop a detailed model of the system, examining the evolution of the internal state of the atom as well as the centre-of-mass motion of the atom in the trap. In particular we are interested in the regime where the atom is high up in the trapping potential, excited far above the ground state. This type of system has not been thoroughly investigated in the highly excited regime.

1.1 Outline

In the following three chapters we review some of the theory that will be used to develop our model. We begin in Chapter 2 with the standard treatment of a stationary two-level atom driven near resonance by a classical electromagnetic field. In Chapter 3 we review two popular techniques used in the treatment of open quantum systems. A spontaneously emitting two-level atom in free space is used as an example system. In Chapter 4 the two ideas are combined to obtain the theory of resonance fluorescence.

The original content of this thesis begins in Chapter 5, where we introduce our model. We give a qualitative explanation for the results that are obtained, and discuss the validity of the approximations used. The system is analysed in more detail in Chapter 6, where we give some quantitative calculations and a discussion of the parameter dependence of the system. In Chapter 7 we simplify the model further so that we can analyse features of the motion that would otherwise take too long to compute. We conclude in Chapter 8 with a summary of the results and a discussion of the avenues for future research.

Chapter 2

Interaction of an Atom with a Coherent Electromagnetic Field

In this chapter we introduce one of the fundamental systems in quantum optics: a two-level atom interacting with a coherent electromagnetic field. The field is a monochromatic classical wave which is near resonance with the atomic transition - in practice this can be provided by a laser. Because the laser field is monochromatic, the Einstein rate equation approach (in terms of absorption and stimulated emission) is inadequate. Rather than jump between the two atomic states, we look at a continuous evolution of the superposition of both. To begin with we neglect spontaneous emission, leaving it to the next chapter.

2.1 The Two-Level Atom

We consider as a basis for our atomic system two energy eigenstates: an excited state $|2\rangle$ with energy E_2, and a ground state $|1\rangle$ with energy E_1. By restricting ourselves to only two energy states we are anticipating a driving field that is near resonance with this transition, and far from resonance with all others. In that case, the internal motion of the atom consists only of transitions between these two states; probabilities for other transitions are vanishingly small. The Hamiltonian of the system can be expanded as

$$\begin{aligned} H_0 &= E_1 |1\rangle \langle 1| + E_2 |2\rangle \langle 2| \\ &= \frac{1}{2}(E_1 + E_2)\hat{1} + \frac{1}{2}(E_2 - E_1)\sigma_z, \end{aligned} \tag{2.1}$$

where $\hat{1}$ is the identity operator and σ_z is defined as

$$\sigma_z \equiv |2\rangle \langle 2| - |1\rangle \langle 1| . \tag{2.2}$$

The first term in (2.1) is a constant which can be removed by setting the zero of energy half way between E_1 and E_2. If we let $E_2 - E_1 = \hbar\omega_A$, the Hamiltonian can be written as

$$H_0 = \frac{1}{2}\hbar\omega_A\sigma_z. \tag{2.3}$$

A schematic of the energy level structure is shown in Fig. 2.1. We also introduce the raising and lowering operators

$$\sigma_- \equiv |1\rangle \langle 2| , \qquad \sigma_+ \equiv |2\rangle \langle 1| . \tag{2.4}$$

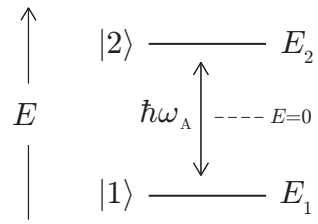

Fig. 2.1: Energy levels of the two-level atom.

The action of the raising and lowering operators follows directly from the orthonormality of the basis states. It is also interesting to consider the sums and differences of the raising and lowering operators given by

$$\begin{aligned} \sigma_x &= (\sigma_+ + \sigma_-) \\ \sigma_y &= -i\,(\sigma_+ - \sigma_-)\,, \end{aligned} \tag{2.5}$$

as σ_x, σ_y and σ_z are mathematically identical to the Pauli spin operators used in spin-$\frac{1}{2}$ systems. In the context of a two-level atom they are referred to as pseudo-spin operators since the two levels are not associated with physical spin states. The commutation relations of the atomic operators are

$$[\sigma_+, \sigma_-] = \sigma_z, \qquad [\sigma_\pm, \sigma_z] = \mp 2\sigma_\pm. \tag{2.6}$$

2.2 The Interaction Hamiltonian

The driving field at position $\boldsymbol{r}$ and time t is characterised by the classical electric field vector

$$\boldsymbol{E}(\boldsymbol{r}, t) = \hat{\boldsymbol{e}}_0 E_0 \cos(\omega t - \boldsymbol{k}\cdot\boldsymbol{r} + \phi_0)\,, \tag{2.7}$$

where E_0 is the field amplitude, $\boldsymbol{k}$ and ω are the wavevector and frequency of the electromagnetic wave, respectively, $\hat{\boldsymbol{e}}_0$ is the unit polarization vector, and ϕ_0 is a constant phase.

When an atom is placed in this electric field, its electronic charge distribution is distorted. If the electric field is constant over the space occupied by the atom, this distortion is characterised by the dipole interaction. We write

$$\boldsymbol{E}(t) = \hat{\boldsymbol{e}}_0 E_0 \cos(\omega t + \phi_0)\,, \tag{2.8}$$

where the constant $\boldsymbol{k}\cdot\boldsymbol{r}$ term has been absorbed into the phase ϕ_0. This is called the *dipole approximation*. The assumption that the electric field is constant across the atom is justified at optical frequencies, where the wavelengths are around 1000 times larger than the diameter of an atom. The dipole moment operator for our atom is

$$\boldsymbol{d} = -e\sum_{j=1}^{Z} \boldsymbol{r}_j, \tag{2.9}$$

where e is the electronic charge, $\boldsymbol{r}_j$ are the position operators for each electron, and the summation is over all electrons in the atom. The dipole operator can be expanded in terms

of the atomic energy eigenstates as

$$\boldsymbol{d} = \sum_{n,m=1}^{2} \boldsymbol{\mu}_{nm} \left|n\right\rangle \left\langle m\right|, \tag{2.10}$$

where we introduce the atomic dipole matrix elements

$$\boldsymbol{\mu}_{nm} = -e \sum_{j=1}^{Z} \left\langle n\right| \boldsymbol{r}_j \left|m\right\rangle. \tag{2.11}$$

Things can be simplified further by noting that, due to symmetry considerations, the energy eigenstates cannot have a permanent dipole moment,[1] that is

$$\left\langle n\right| \boldsymbol{r}_j \left|n\right\rangle = 0. \tag{2.12}$$

The dipole operator becomes

$$\boldsymbol{d} = \boldsymbol{\mu}_{12}\sigma_- + \boldsymbol{\mu}_{21}\sigma_+, \tag{2.13}$$

where the atomic raising and lowering operators have been introduced using (2.4).

Classically, the interaction energy of a dipole moment $\boldsymbol{d}$ in the presence of an electric field $\boldsymbol{E}$ is given by

$$U = -\boldsymbol{d} \cdot \boldsymbol{E}, \tag{2.14}$$

so the interaction Hamiltonian in the dipole approximation is

$$H_I = -E_0 \cos(\omega t + \phi_0) \left(\mu_{12}\sigma_- + \mu_{21}\sigma_+\right), \tag{2.15}$$

where

$$\mu_{nm} = \boldsymbol{\mu}_{nm} \cdot \hat{\boldsymbol{e}}_0. \tag{2.16}$$

To apply our next approximation we transform into the interaction picture, using (2.3) for our free Hamiltonian H_0. There is also a free Hamiltonian for the field, but in our classical treatment it is a constant which can be neglected; the field is set by equation (2.7) and does not change through the interaction with the atom. State evolution in the interaction picture is governed by the Hamiltonian

$$\begin{aligned} \tilde{H}_I &= \left(e^{\frac{1}{2}i\omega_A\sigma_z t}\right) H_I \left(e^{-\frac{1}{2}i\omega_A\sigma_z t}\right) \\ &= -\frac{E_0}{2}\left\{\mu_{12}\sigma_- \left[e^{-i(\omega_A+\omega)t}e^{-i\phi_0} + e^{-i(\omega_A-\omega)t}e^{i\phi_0}\right]\right. \\ &\quad \left.\mu_{21}\sigma_+ \left[e^{i(\omega_A+\omega)t}e^{i\phi_0} + e^{i(\omega_A-\omega)t}e^{-i\phi_0}\right]\right\}. \end{aligned} \tag{2.17}$$

In transforming operators into the interaction picture we have made use of the Baker-Hausdorff formula

$$e^{iG\lambda} A\, e^{-iG\lambda} = A + i\lambda\,[G, A] + \left(\frac{i^2\lambda^2}{2!}\right)[G, [G, A]] + ..., \tag{2.18}$$

[1] See [14] pp. 260 for a discussion.

where A and G are operators and λ is a parameter.[2] At optical frequencies the $e^{\pm i(\omega_A+\omega)t}$ terms in (2.17) oscillate much more rapidly than the $e^{\pm i(\omega_A-\omega)t}$ terms, so during the evolution they will average to zero. By neglecting these terms we are making the *rotating wave approximation*.[3] Switching back into the Schrödinger picture, we arrive at

$$H_I = -\frac{E_0}{2}\left\{\mu_{12}\sigma_- e^{i(\omega t+\phi_0)} + \mu_{21}\sigma_+ e^{-i(\omega t+\phi_0)}\right\}. \tag{2.19}$$

The phase ϕ_0 and the phase of the atomic dipole matrix elements are arbitrary. They can be absorbed into the definitions of the raising and lowering operators. This allows us to rewrite the interaction Hamiltonian as

$$H_I = \hbar\frac{\Omega}{2}\left\{\sigma_- e^{i\omega t} + \sigma_+ e^{-i\omega t}\right\}, \tag{2.20}$$

where the interaction energy is characterised by the Rabi frequency

$$\Omega = \frac{E_0}{\hbar}\left|\mu_{12}\right| = \frac{E_0}{\hbar}\left|\mu_{21}\right|. \tag{2.21}$$

2.3 Rabi Oscillation

The state of the atom in the interaction picture is represented by the ket

$$\left|\psi(t)\right\rangle = \tilde{c}_1(t)\left|1\right\rangle + \tilde{c}_2(t)\left|2\right\rangle. \tag{2.22}$$

Applying the Schrödinger equation using Hamiltonian (2.20) in the interaction picture, we arrive at the system of coupled differential equations

$$\frac{d\tilde{c}_1}{dt} = -i\frac{\Omega}{2}e^{i\Delta\omega t}\tilde{c}_2, \tag{2.23a}$$

$$\frac{d\tilde{c}_2}{dt} = -i\frac{\Omega}{2}e^{-i\Delta\omega t}\tilde{c}_1, \tag{2.23b}$$

where $\Delta\omega = \omega - \omega_A$ is the detuning of the driving field from the atomic transition. Supposing the atom is in the ground state at $t = 0$, we solve these equations for the probability to find the atom in the excited state at time t

$$\left|\tilde{c}_2(t)\right|^2 = \frac{1}{2}\left(\frac{\Omega}{\Omega'}\right)^2\left[1-\cos\left(\Omega' t\right)\right], \tag{2.24}$$

where we have introduced the generalised Rabi frequency

$$\Omega' = \sqrt{\left(\Delta\omega\right)^2 + \Omega^2}. \tag{2.25}$$

The state of the atom oscillates sinusoidally between the excited and ground states with frequency Ω', as shown in Fig. 2.2. This is known as Rabi oscillation. Note that only if the system is at resonance ($\Delta\omega = 0$) do the oscillations go all the way up to $\left|\tilde{c}_2\right|^2 = 1$. In the system we will study in this thesis, the atom exhibits more complex behaviour than simple Rabi oscillation. However, the structure introduced here will be useful in our analysis.

[2] A derivation of this formula can be found in [15] pp. 39.

[3] In this thesis we will consider detunings of up to 10^7Hz, while the frequencies themselves are 10^{15}Hz, so the rotating wave approximation is a valid one.

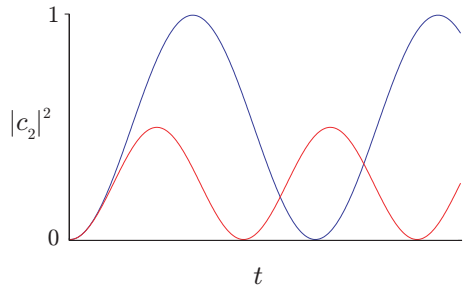

Fig. 2.2: Rabi oscillation at resonance (blue line), and with a detuning $\Delta\omega = \Omega$ (red line).

2.4 Optical Bloch Equations

The optical Bloch equations are a convenient way to represent the dynamics of any two-state system. They were originally developed for magnetic resonance systems where the two-state system is a spin driven by a magnetic field [16]. In the present case our system is the two-dimensional Hilbert space of quantum states available to the atom. The state of the system in the Schrödinger picture is

$$|\psi(t)\rangle = c_1(t)\,|1\rangle + c_2(t)\,|2\rangle\,. \tag{2.26}$$

We define the Bloch vector by

$$\boldsymbol{m} = \begin{bmatrix} u \\ v \\ w \end{bmatrix} = \begin{bmatrix} c_1 c_2^* + c_1^* c_2 \\ -i\left(c_1 c_2^* - c_1^* c_2\right) \\ |c_2|^2 - |c_1|^2 \end{bmatrix}. \tag{2.27}$$

Since the Bloch vector is a normalised vector in $\mathbb{R}^3$ $(u^2 + v^2 + w^2 = 1)$ we can represent it by a point on the surface of a unit sphere, as shown in Fig. 2.3 (a). This unit sphere is called the Bloch sphere. Note that the Bloch vector is completely characterised by the two angles θ and ϕ. This is because the complex numbers c_1 and c_2 that characterise the quantum state are normalised $(|c_1|^2 + |c_2|^2 = 1)$ and the overall phase is arbitrary. The time evolution of the Bloch vector follows from (2.23), leading to the optical Bloch equations (in the rotating wave approximation)

$$\frac{du}{dt} = -\omega_A v + 2w\Omega \sin(\omega t)\,, \tag{2.28a}$$

$$\frac{dv}{dt} = \omega_A u + 2w\Omega \cos(\omega t)\,, \tag{2.28b}$$

$$\frac{dw}{dt} = \Omega\left[v\cos(\omega t) - u\sin(\omega t)\right]. \tag{2.28c}$$

These equations can be solved by introducing the new variables

$$u' = u\sin(\omega t) - v\cos(\omega t)\,, \tag{2.29a}$$

$$v' = -u\cos(\omega t) - v\sin(\omega t)\,, \tag{2.29b}$$

leading to new equations of motion

$$\frac{du'}{dt} = -\Delta\omega v' + \Omega w, \tag{2.30a}$$

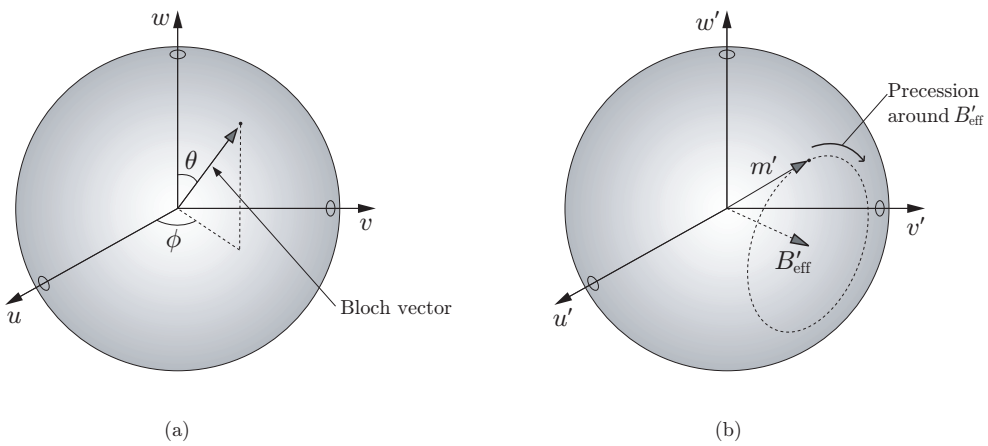

Fig. 2.3: (a) The Bloch sphere. (b) Motion of the Bloch vector.

$$\frac{dv'}{dt} = \Delta\omega u', \tag{2.30b}$$

$$\frac{dw}{dt} = -\Omega u. \tag{2.30c}$$

We rewrite these equations as a vector cross product

$$\frac{d\boldsymbol{m}'}{dt} = \boldsymbol{B}'_{\text{eff}} \times \boldsymbol{m}', \tag{2.31}$$

where

$$\boldsymbol{m}' = \begin{bmatrix} u' \\ v' \\ w' \end{bmatrix}, \qquad \boldsymbol{B}'_{\text{eff}} = \begin{bmatrix} 0 \\ \Omega \\ \Delta\omega \end{bmatrix}. \tag{2.32}$$

The evolution of the Bloch vector is analagous to that of a magnetic moment $\boldsymbol{m}'$ in a static magnetic field $\boldsymbol{B}'_{\text{eff}}$. The direction of change in $\boldsymbol{m}'$ is perpendicular to both $\boldsymbol{m}'$ and $\boldsymbol{B}'_{\text{eff}}$, so $\boldsymbol{m}'$ precesses around $\boldsymbol{B}'_{\text{eff}}$, as shown in Fig. 2.4 (b). The precession of the Bloch vector is just another way of looking at the Rabi oscillation encountered in Section 1.3 — the precession frequency is the magnitude of $\boldsymbol{B}'_{\text{eff}}$, which is identical to the generalised Rabi frequency given by equation (2.25). The description in terms of motion on the Bloch sphere will be useful when studying the system that is the subject of this thesis.

Chapter 3

Spontaneous Emission

The driven two-level atom is a simple system, but complications arise when spontaneous emission is considered. When photons are spontaneously emitted they leave the atom for good; keeping track of every one of these photons is unnecessary. It seems more fitting to say that once a photon is spontaneously emitted has left the system, and is no longer part of our description. This is an example of an open (or dissipative) system, where information is lost to the environment. In this chapter we introduce a few central concepts in the quantum theory of open systems and discuss how to treat such environmental losses, using the two-level atom as a specific example.

3.1 Mixed States and Density Operators

The pure state of a quantum mechanical system is what we represent (in the Schrödinger picture) with a state ket. Given an initial pure state and a system Hamiltonian, the state at a later time is completely determined; it is our ability to measure physical observables from this state that is restricted by Heisenberg's uncertainty principle. However, we can treat systems where there is a classical uncertainty in the state itself. For example, consider a collection of particles where 40% are in state $|a\rangle$ and 60% are in state $|b\rangle$. The average measured value of an observable A is just the ensemble average over both states:

$$[A] = \frac{4}{10}\langle a|A|a\rangle + \frac{6}{10}\langle b|A|b\rangle. \tag{3.1}$$

Note that this expression contains two types of averages: the quantum mechanical average (expectation value) of an operator A in a given state, and the a classical average over a range of states. We define the density operator for the system as

$$\rho = \frac{4}{10}|a\rangle\langle a| + \frac{6}{10}|b\rangle\langle b|. \tag{3.2}$$

This is called a mixed state, because it represents a mixture of pure states with different statistical weightings. The ensemble average can then be expressed as

$$\begin{aligned}[A] &= \frac{4}{10}\langle a|A|a\rangle + \frac{6}{10}\langle b|A|b\rangle \\ &= \mathrm{tr}\left\{\frac{4}{10}\langle a|A|a\rangle + \frac{6}{10}\langle b|A|b\rangle\right\}\end{aligned}$$

$$
\begin{aligned}
&= \operatorname{tr}\left\{\frac{4}{10}|a\rangle\langle a|A + \frac{6}{10}|b\rangle\langle b|A\right\} \\
&= \operatorname{tr}\{\rho A\}\,, \qquad (3.3)
\end{aligned}
$$

where the cyclic property of the trace has been applied ($\operatorname{tr}\{AB\} = \operatorname{tr}\{BA\}$). The trace operation is representation independent, so the expectation value can be evaluated in any convenient basis.

In general, the density operator for a mixed state is the sum over all pure states $|\psi_i\rangle$ with weighting w_i:

$$
\rho = \sum_i w_i |\psi_i\rangle\langle\psi_i|. \qquad (3.4)
$$

The time evolution of the density operator follows from the Schrödinger equation:

$$
\begin{aligned}
\frac{d\rho}{dt} &= \sum_i w_i \left(\frac{d|\psi_i\rangle}{dt}\langle\psi_i| + |\psi_i\rangle\frac{d\langle\psi_i|}{dt}\right) \\
&= \frac{1}{i\hbar}\sum_i w_i \left(H|\psi_i\rangle\langle\psi_i| - |\psi_i\rangle\langle\psi_i|H\right) \\
&= \frac{1}{i\hbar}\left[H, \rho\right]. \qquad (3.5)
\end{aligned}
$$

The density operator formalism outlined above is useful when treating dissipative systems, as states that are initially pure do not generally remain so.

3.2 The Master Equation

When a system interacts with its environment, information is lost and classical uncertainty is introduced. We approach this problem by considering the system and environment as a single composite system and averaging away the states of the environment. What we are left with is, in general, a mixed state represented by a density operator, and the master equation governs the time evolution of this state. Exactly how the state can be viewed as a statistical mixture of pure states may be unclear, but in the next section we will see that quantum trajectory theory provides a decomposition with a simple physical interpretation. In this section we outline a derivation of the master equation for a radiatively damped two-level atom.[1]

3.2.1 Reduced Density Operator

We consider a system S interacting with an environment represented by a reservoir R. The aim is to obtain an equation of motion for S with the properties of R entering as parameters; we are not interested in the evolution of R itself. The Hamiltonian for the composite system $S \otimes R$ is

$$
H = H_S + H_R + H_{SR}, \qquad (3.6)
$$

[1] Here we only summarise the derivation, for a more thorough treatment see [17] pp. 1-16, 30-32. In particular the Markov approximation is justified formally, and a reservoir at a finite temperature is considered.

where H_S and H_R are Hamiltonians for the system and reservoir, and H_{SR} is an interaction Hamiltonian. We define $\chi(t)$ as the density operator for $S \otimes R$. From (3.5) the composite system evolves according to

$$\frac{d\chi}{dt} = \frac{1}{i\hbar}\left[H, \chi\right]. \tag{3.7}$$

We introduce the reduced density operator $\rho(t)$, defined by

$$\rho(t) \equiv \mathrm{tr}_R\left\{\chi(t)\right\}, \tag{3.8}$$

where the trace operation projects onto the Hilbert space of S by averaging over the states of R. An operator $\hat{A}$ in the Hilbert space of S can be averaged with knowledge of $\rho(t)$ alone:

$$\left\langle \hat{A} \right\rangle = \mathrm{tr}_{S\otimes R}\left\{\hat{A}\chi(t)\right\} = \mathrm{tr}_S\left\{\hat{A}\mathrm{tr}_R[\chi(t)]\right\} = \mathrm{tr}_S\left\{\hat{A}\rho(t)\right\}, \tag{3.9}$$

so the reduced density operator contains all information we need to describe S.

3.2.2 Born and Markov Approximations

Our next step is to recast equation (3.7) into a form where some approximations can be made. What follows is essentially perturbation theory and, in the context of a two level atom with radiative damping, is physically equivalent to the Wigner-Weisskopf theory of natural linewidth. First we transform into the interaction picture, defining

$$\tilde{\chi}(t) \equiv e^{(i/\hbar)(H_S+H_R)t}\chi(t)e^{(-i/\hbar)(H_S+H_R)t}. \tag{3.10}$$

We trace over the reservoir states to find

$$\mathrm{tr}_R\left\{\tilde{\chi}(t)\right\} = e^{(i/\hbar)H_S t}\mathrm{tr}_R\left\{\chi(t)\right\}e^{(-i/\hbar)H_S t} \equiv \tilde{\rho}(t). \tag{3.11}$$

The time derivative of $\tilde{\chi}(t)$ follows from (3.6) and (3.7):

$$\dot{\tilde{\chi}} = \frac{1}{i\hbar}\left[\tilde{H}_{SR}(t), \tilde{\chi}\right], \tag{3.12}$$

where $\tilde{H}_{SR}(t)$ is given by

$$\tilde{H}_{SR}(t) = e^{(i/\hbar)(H_S+H_R)t}H_{SR}e^{(-i/\hbar)(H_S+H_R)t}. \tag{3.13}$$

Integrating (3.12) formally gives

$$\tilde{\chi}(t) = \chi(0) - \frac{1}{i\hbar}\int_0^t dt'[\tilde{H}_{SR}(t'), \tilde{\chi}(t')], \tag{3.14}$$

which we substitute into (3.12) to get

$$\dot{\tilde{\chi}} = \frac{1}{i\hbar}[\tilde{H}_{SR}(t), \chi(0)] - \frac{1}{\hbar^2}\int_0^t dt'[\tilde{H}_{SR}(t), [\tilde{H}_{SR}(t'), \tilde{\chi}(t')]]. \tag{3.15}$$

At this point we assume that before $t = 0$ the system and reservoir did not interact and thus were uncorrelated. The initial state of the combined system $\chi(0)$ must factorise as

$$\chi(0) = \rho(0)R_0, \tag{3.16}$$

where R_0 is the initial density operator for the reservoir. Taking the trace over (3.15) and using (3.11) we arrive at a general form of the master equation

$$\dot{\tilde{\rho}} = -\frac{1}{\hbar^2}\int_0^t dt' \mathrm{tr}_R \left\{ [\tilde{H}_{SR}(t), [\tilde{H}_{SR}(t'), \tilde{\chi}(t')]] \right\}, \tag{3.17}$$

where we have assumed that $\mathrm{tr}_R[\tilde{H}_{SR}(t)R_0] = 0$, a condition that can be arranged by adding $\mathrm{tr}_R\{H_{SR}R_0\}$ to the system Hamiltonian. We can substitute $\tilde{\chi}(t') = \tilde{\rho}(t')R_0$ into (3.17), neglecting any higher order terms in H_{SR}. This is referred to as the Born approximation because of its similarity to an approximation encountered in scattering theory.[2] It is valid when the reservoir is only slightly perturbed by its interaction with the system. The resulting equation is

$$\dot{\tilde{\rho}} = -\frac{1}{\hbar^2}\int_0^t dt' \mathrm{tr}_R \left\{ [\tilde{H}_{SR}(t), [\tilde{H}_{SR}(t'), \tilde{\rho}(t')R_0]] \right\}. \tag{3.18}$$

Furthermore, we can assume that the evolution of $\tilde{\rho}(t)$ depends primarily on its current value, rather than its past history - this is the Markov approximation. We incorporate this by replacing $\tilde{\rho}(t')$ in the integrand with $\tilde{\rho}(t)$. If the reservoir is a large system close to thermal equilibrium, perturbations of the reservoir by the system quickly die away, where 'quickly' is relative to the timescale at which the system itself evolves. In this case the history of the system has a negligible effect on the future evolution and the Markov approximation is valid. We arrive at the master equation in the Born-Markov approximation:

$$\dot{\tilde{\rho}} = -\frac{1}{\hbar^2}\int_0^t dt' \mathrm{tr}_R \left\{ [\tilde{H}_{SR}(t), [\tilde{H}_{SR}(t'), \tilde{\rho}(t)R_0]] \right\}. \tag{3.19}$$

3.2.3 The Master Equation for a Two-Level Atom

We now consider a specific system: the radiatively damped two-level atom. The reservoir in this case is a collection of harmonic oscillators, representing the modes of the vacuum radiation field which the atom spontaneously emits into. The Hamiltonian of the composite system, in the rotating-wave and dipole approximations, is composed of[3]

$$H_S \equiv \frac{1}{2}\hbar\omega_A\sigma_z, \tag{3.20a}$$

$$H_R \equiv \sum_{\boldsymbol{k},\lambda} \hbar\omega_k r^\dagger_{\boldsymbol{k},\lambda} r_{\boldsymbol{k},\lambda}, \tag{3.20b}$$

$$H_{SR} \equiv \sum_{\boldsymbol{k},\lambda} \hbar\left(\kappa^*_{\boldsymbol{k},\lambda} r^\dagger_{\boldsymbol{k},\lambda}\sigma_- + \kappa_{\boldsymbol{k},\lambda} r_{\boldsymbol{k},\lambda}\sigma_+\right), \tag{3.20c}$$

where $r^\dagger_{\boldsymbol{k},\lambda}$ and $r_{\boldsymbol{k},\lambda}$ are the creation and annihilation operators for the reservoir mode with wavevector $\boldsymbol{k}$, frequency ω_k, and polarization state λ. These operators have the commutation relations

$$\left[r_i, r_j^\dagger\right] = \delta_{ij}, \qquad \left[r_i^\dagger, r_j^\dagger\right] = 0, \qquad [r_i, r_j] = 0. \tag{3.21}$$

[2] An introduction to the Born approximation in scattering theory can be found in [14], Section 7.2.

[3] This is an extension of the treatment in Section 2.2 to a quantised electromagnetic field containing many modes. A justification of the Hamiltonian can be found in [18] pp. 27-30.

The dipole coupling constant for this field mode is given by

$$\kappa_{\boldsymbol{k},\lambda} \equiv -ie^{i\boldsymbol{k}\cdot\boldsymbol{r}_A}\sqrt{\frac{\omega_k}{2\hbar\epsilon_0 V}}\hat{e}_{\boldsymbol{k},\lambda}\cdot\boldsymbol{\mu}_{21}. \tag{3.22}$$

Applying the Baker-Hausdorff formula to both the atomic operators and the field operators, we transform H_{SR} into the interaction picture to get

$$\tilde{H}_{SR}(t) = \hbar\sum_{\boldsymbol{k},\lambda}\left[\kappa^*_{\boldsymbol{k},\lambda}r^\dagger_{\boldsymbol{k},\lambda}e^{i(\omega_k-\omega_A)t}\sigma_- + \kappa_{\boldsymbol{k},\lambda}r_{\boldsymbol{k},\lambda}e^{-i(\omega_k-\omega_A)t}\sigma_+\right], \tag{3.23}$$

using the fact that operators from different reservoir modes commute. The next step is to insert this into (3.19) and take the operators in S outside the trace. The trace can then be evaluated using the Fock states of the reservoir as a basis. Because (3.19) contains two nested commutators we have an equation with 16 terms, but most of these vanish as the reservoir is assumed to be in the vacuum state and the traces are zero.[4] We are left with

$$\begin{aligned}\dot{\tilde{\rho}} = -\int_0^t dt'\sum_{\boldsymbol{k},\lambda}|\kappa_{\boldsymbol{k},\lambda}|^2\Big\{&e^{i(\omega_A-\omega_k)(t-t')}\left[\sigma_+\sigma_-\tilde{\rho}-\sigma_-\tilde{\rho}\sigma_+\right]\\ &+e^{-i(\omega_A-\omega_k)(t-t')}\left[\tilde{\rho}\sigma_+\sigma_- - \sigma_-\tilde{\rho}\sigma_+\right]\Big\}.\end{aligned} \tag{3.24}$$

Now we can convert the summation over reservoir frequencies to an integral, introducing a density of states $g(\boldsymbol{k})$ so that the number of oscillators in the interval from k to $k+dk$ is $g(\boldsymbol{k})d^3k$. We then change variables to $\tau = t-t'$ and find

$$\begin{aligned}\dot{\tilde{\rho}} = -\int_0^t d\tau\sum_\lambda\int d^3k\; g(\boldsymbol{k})\,|\kappa_\lambda(\boldsymbol{k})|^2\Big\{&e^{i(\omega_A-kc)\tau}\left[\sigma_+\sigma_-\tilde{\rho}-\sigma_-\tilde{\rho}\sigma_+\right]\\ &+e^{-i(\omega_A-kc)\tau}\left[\tilde{\rho}\sigma_+\sigma_- - \sigma_-\tilde{\rho}\sigma_+\right]\Big\}.\end{aligned} \tag{3.25}$$

Under the Markov approximation, if $\tau > t$ the $e^{\pm i(\omega_A-kc)\tau}$ terms oscillate rapidly with k and the integral over k is small. This means we can extend the integral over τ to infinity. We can then evaluate the τ integral using

$$\lim_{t\to\infty}\int_0^t d\tau e^{i(\omega_A-\omega)\tau} = \pi\delta(\omega_A-\omega) + i\frac{P}{\omega_A-\omega}, \tag{3.26}$$

where P denotes the Cauchy principle value. Equation (3.25) becomes

$$\dot{\tilde{\rho}} = \left(\frac{\gamma}{2}+i\Delta\right)(\sigma_-\tilde{\rho}\sigma_+ - \sigma_+\sigma_-\tilde{\rho}) + \left(\frac{\gamma}{2}-i\Delta\right)(\sigma_-\tilde{\rho}\sigma_+ - \tilde{\rho}\sigma_+\sigma_-), \tag{3.27}$$

where

$$\gamma \equiv 2\pi\sum_\lambda\int d^3k\;\delta(kc-\omega_A)g(\boldsymbol{k})\,|\kappa_\lambda(\boldsymbol{k})|^2, \tag{3.28}$$

$$\Delta \equiv \sum_\lambda P\int d^3k\;\frac{g(\boldsymbol{k})\,|\kappa_\lambda(\boldsymbol{k})|^2}{\omega_A-kc}. \tag{3.29}$$

[4]This is not a bad approximation in practice because at optical frequencies $\hbar\omega_A >> k_BT$ and thermal effects are negligible.

Using the properties of the atomic raising and lowering operators

$$\sigma_+\sigma_- = \frac{1}{2}(1+\sigma_z), \qquad \sigma_-\sigma_+ = \frac{1}{2}(1-\sigma_z), \tag{3.30}$$

we rewrite (3.27) as

$$\dot{\tilde{\rho}} = -\frac{i\Delta}{2}\left[\sigma_z, \tilde{\rho}\right] + \frac{\gamma}{2}\left(2\sigma_-\tilde{\rho}\sigma_+ - \sigma_+\sigma_-\tilde{\rho} - \tilde{\rho}\sigma_+\sigma_-\right). \tag{3.31}$$

Finally, we transform back into the Schrödinger picture to get the master equation for a radiatively damped two-level atom in a vacuum reservoir:

$$\dot{\rho} = -i\frac{1}{2}\left(\omega_A + \Delta\right)\left[\sigma_z, \rho\right] + \frac{\gamma}{2}\left(2\sigma_-\rho\sigma_+ - \sigma_+\sigma_-\rho - \rho\sigma_+\sigma_-\right). \tag{3.32}$$

The Δ term here is the Lamb shift, but since we have used an interaction Hamiltonian in the rotating wave approximation it does not give the correct result.[5] In practice the Lamb shift is absorbed into the transition frequency as that is usually what is measured.

3.3 Quantum Trajectory Theory

The master equation is a popular and well established tool used in the treatment of dissipative quantum systems. However, in this thesis we use a different approach, known as quantum trajectory theory. We have introduced the master equation so that we can derive quantum trajectory theory from it, but in principle it is an alternative approach and can be derived using other means. In this section we introduce quantum trajectory theory via our two-level atom system, for a more rigorous and formal introduction to the theory see [19], Lectures 7-10.

3.3.1 Quantum Trajectories for a Two-Level Atom

We return to the example of a two-level atom. Suppose it is in a vacuum, and is initially in the excited state. If we represent the atom with a density operator, we can view it as the mixed state

$$\rho(t) = w_1(t)\left|1\right\rangle\left\langle 1\right| + w_2(t)\left|2\right\rangle\left\langle 2\right|, \tag{3.33}$$

where $w_1(0) = 0$ and $w_2(0) = 1$. The master equation in this case tells us how the weightings $w_i(t)$ change with time. It is important to point out that the decomposition of $\rho(t)$ in terms of energy eigenstates is arbitrary, we could expand it in another basis if we chose to. However, we can give some physical significance to this particular decomposition. Suppose the atom is surrounded by an array of photodetectors. After some time, one of the detectors will click and we know that a photon has been emitted. The atom is now in the ground state. This act of measurement tells us that the pure state evolution was

$$\left|\psi(t)\right\rangle = \left|2\right\rangle, \qquad \text{for } t < t_0,$$

[5] There are actually two reasons why it does not give the correct result. We can easily account for the rotating wave approximation (see [17] pp. 32 for a discussion) but in this case relativistic corrections are also necessary for agreement with experiment.

$$|\psi(t)\rangle = |1\rangle\,, \qquad \text{for } t > t_0, \tag{3.34}$$

where t_0 was the time that the photon was emitted.[6] This pure state evolution with a jump at t_0 is an example of a quantum trajectory. We can perform this experiment many times, averaging these trajectories to recover the weightings $w_i(t)$.

Of course, the initial state does not have to be an energy eigenstate — we could choose the general coherent superposition

$$|\psi(0)\rangle = c_1\,|1\rangle + c_2\,|2\rangle\,. \tag{3.35}$$

The coefficients c_i will now vary as the state evolves. If a photon is detected, we know that the atom has collapsed to the ground state, where it will stay. However, a photon may never be emitted as the atom was not definitely excited to begin with. After a long time the system can decay to the ground state through the continuous evolution, without ever making a quantum jump.

We can quantify the trajectory evolution by looking at the master equation (3.32). Absorbing the Lamb shift into the transition frequency, we have

$$\dot{\rho} = -i\frac{1}{2}\omega_A\,[\sigma_z, \rho] + \frac{\gamma}{2}\left(2\sigma_-\rho\sigma_+ - \sigma_+\sigma_-\rho - \rho\sigma_+\sigma_-\right). \tag{3.36}$$

The only term that causes jumps from energy eigenstates is the $2\sigma_-\rho\sigma_+$ term. This motivates the definition of the superoperators

$$\begin{aligned} \mathcal{L}_B &\equiv -i\left[\frac{1}{2}\omega_A\sigma_z, \cdot\right] - \frac{\gamma}{2}\left(\sigma_+\sigma_- \cdot + \cdot\,\sigma_+\sigma_-\right), \\ \mathcal{L}_J &\equiv \gamma\sigma_- \cdot \sigma_+, \end{aligned} \tag{3.37}$$

so the master equation can be written as

$$\dot{\rho} = \left(\mathcal{L}_B + \mathcal{L}_J\right)\rho. \tag{3.38}$$

If we write

$$\rho = e^{\mathcal{L}_B t}\bar{\rho}, \tag{3.39}$$

we find $\bar{\rho}$ satisfies the equation of motion

$$\dot{\bar{\rho}} = e^{-\mathcal{L}_B t}\mathcal{L}_J e^{\mathcal{L}_B t}\bar{\rho}. \tag{3.40}$$

We integrate this formally and use (3.39) to get

$$\rho(t) = e^{\mathcal{L}_B t}\rho(0) + \int_0^t dt' e^{\mathcal{L}_B(t-t')}\mathcal{L}_J e^{\mathcal{L}_B t'}\rho(0), \tag{3.41}$$

which is known as the Dyson expansion for the density operator, where $\mathcal{L}_J$ is the interaction term. The integrand in (3.41) has a simple interpretation: an initial state $\rho(0)$ evolves continuously to t', a jump occurs, and the state evolves continuously again up to t. The density operator $\rho(t)$ is unravelled as an integral over trajectories which are the possible outcomes of an experiment where we are constantly looking to see if a jump has occured.

[6] Realistically, we measure the time that the detector goes 'click' and infer t_0 from that measurement, taking into account the time required for the light to travel from the atom to the detector.

To show that the evolution described by $\mathcal{L}_B$ is pure we note that

$$\frac{d\left(|\psi(t)\rangle\langle\psi(t)|\right)}{dt} = \mathcal{L}_B\left(|\psi(t)\rangle\langle\psi(t)|\right) \;\Rightarrow\; \frac{d\,|\psi(t)\rangle}{dt} = \frac{1}{i\hbar}H_{\text{eff}}\,|\psi(t)\rangle\,, \tag{3.42}$$

if we introduce the non-Hermitian Hamiltonian

$$H_{\text{eff}} = \frac{1}{2}\hbar\omega_A\sigma_z - i\hbar\frac{\gamma}{2}\sigma_+\sigma_-. \tag{3.43}$$

The effective Hamiltonian H_{eff} describes a pure state evolution which is not unitary, so normalisation is not preserved. The norm of our atomic state $|\psi(t)\rangle$ evolving under H_{eff} is given by

$$||\psi(t)||^2 = |c_1(t)|^2 + |c_2(t)|^2 \tag{3.44}$$

and represents the *no-jump probability*, the probability to have evolved up to time t without a quantum jump occuring. This is a consistent generalisation from closed systems where the state remains normalised and the no-jump probability is always one. We can interpret the coefficients $|c_i(t)|^2$ as joint probabilities, so $|c_2(t)|^2$ is the probability to be in the excited state and have had no quantum jumps up to time t. We can normalise to get the inferred quantum state

$$\left|\bar{\psi}(t)\right\rangle = \frac{|\psi(t)\rangle}{\sqrt{\langle\psi(t)|\psi(t)\rangle}}. \tag{3.45}$$

Using the same expansion for $|\bar{\psi}(t)\rangle$ we interpret the coefficients $|\bar{c}_i(t)|^2$ as conditional probabilities, so $|\bar{c}_2(t)|^2$ is the probability to be in the excited state given that we have had no quantum jumps up to time t.

We can see the effect of the superoperator $\mathcal{L}_J$ on the pure state $|\psi(t)\rangle$ from

$$\begin{aligned}\mathcal{L}_J\left(|\psi(t)\rangle\langle\psi(t)|\right) &= \gamma\sigma_-\left(|\psi(t)\rangle\langle\psi(t)|\right)\sigma_+ \\ &= |\psi_J(t)\,\rangle\langle\,\psi_J(t)|\,,\end{aligned} \tag{3.46}$$

if $|\psi_J(t)\rangle = \sqrt{\gamma}\sigma_-|\psi(t)\rangle$. This motivates the definition of the jump operator

$$J = \sqrt{\gamma}\sigma_-. \tag{3.47}$$

The probability of a jump occuring between t and $t + dt$ is given by

$$P_J\,dt = \left\langle\bar{\psi}(t)\left|J^\dagger J\right|\bar{\psi}(t)\right\rangle dt, \tag{3.48}$$

which we simply state here. For a justification see [19], Lecture 9.

3.3.2 Generating Trajectories with Monte Carlo Simulations

The quantum trajectory formalism is well suited to computer simulation. We generate sample trajectories using a Monte Carlo algorithm, at each time step asking if a quantum jump will occur or not. For a state $\left|\bar{\psi}_n\right\rangle$ at time t the procedure is as follows:

1. Calculate the probability to collapse in time Δt

$$\mathrm{P} = \left\langle\bar{\psi}_n\left|J^\dagger J\right|\bar{\psi}_n\right\rangle\Delta t.$$

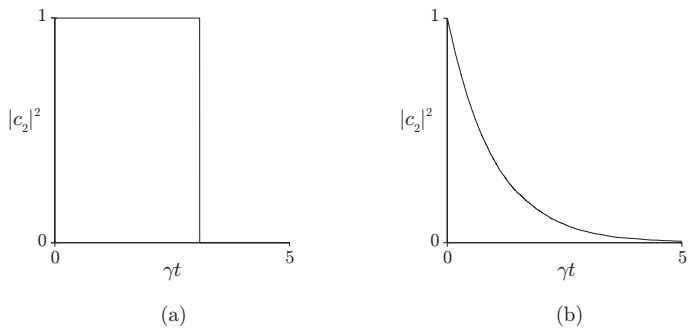

Fig. 3.1: Excitation probability for a two level atom undergoing spontaneous emission, where the atom is initially in the excited state. (a) A single trajectory. (b) An average of 10,000 trajectories.

2. Draw a uniformly distributed random number between 0 and 1

$$r \sim U(0,1).$$

3. If $r > \mathrm{P}$, collapse the state

$$|\psi_{n+1}\rangle = J\left|\bar{\psi}_n\right\rangle.$$

   Otherwise, evolve under H_{eff}

$$\frac{d\,|\psi\rangle}{dt} = -\frac{i}{\hbar}H_{\text{eff}}\,|\psi\rangle\,.$$

4. Normalise the new state

$$\left|\bar{\psi}_{n+1}\right\rangle = \frac{|\psi_{n+1}\rangle}{\sqrt{\langle\psi_{n+1}|\psi_{n+1}\rangle}}.$$

For a two-level atom initially in the excited state, the trajectories are very simple. Since the initial state is an eigenstate of H_{eff}, the atom remains in this state until it jumps. An average over the trajectories recovers the weightings in (3.33), as shown in Fig. 1.1.

3.3.3 Quantum Trajectories in General Systems

In this section we have unravelled the master equation as an integral over trajectories which correspond to possible measurement records. For our two-level atom system we are measuring energy; when a photon is spontaneously emitted and our photodetector clicks, we know that the atom has collapsed to an energy eigenstate. Alternatively, another measurement basis could be used. For example, a homodyne detection system can be arranged to measure the field amplitude of the emitted light, and in this case the decomposition of the master equation is quite different. This particular case is treated in [19], Lecture 9.

Finally, in a general dissipative system many quantum jumps can occur. In the same way as (3.41) the density operator for this more general system can be expanded as a sum over trajectories:

$$\rho(t) = \sum_{n=0}^{\infty}\int_0^t dt_n \int_0^{t_n} dt_{n-1} ... \int_0^{t_2} dt_1 e^{\mathcal{L}_B(t-t_n)}\mathcal{L}_J e^{\mathcal{L}_B(t_n-t_{n-1})}\mathcal{L}_J ... e^{\mathcal{L}_B t_1}\rho(0). \tag{3.49}$$

In this case the same idea applies: at each time the system can jump (according to J) or evolve continuously (according to H_{eff}). A two-level atom driven by an external electromagnetic field, for instance, will not stay in the ground state after it jumps, so the atom will spontaneously emit many times. We will consider such a system in the next chapter.

Chapter 4

Resonance Fluorescence

We now consider a spontaneously emitting two-level atom in the presence of a coherent driving field, combining the ideas from the previous two chapters. Photons from the driving field are absorbed by the atom and reradiated, either back into the laser mode or into the many modes of the vacuum field via spontaneous emission. Since the driving field is near resonance with the atomic transition this 'scattering' process is called resonance fluorescence.

4.1 The Scattered Field

The laser mode is highly populated (containing many photons) and is only slightly perturbed by the interaction with the atom. This is what allows us to treat the driving field classically. The reservoir, however, is initially in the vacuum state, and a fully quantised treatment of the scattered field is required. The Hamiltonian for the composite system $S \otimes R$ is the same as (3.20a), except that H_S obtains an interaction term given by (2.20):

$$H_S \equiv \frac{1}{2}\hbar\omega_A\sigma_z + \hbar\frac{\Omega}{2}\left\{\sigma_- e^{i\omega_A t} + \sigma_+ e^{-i\omega_A t}\right\}, \tag{4.1a}$$

$$H_R \equiv \sum_{\boldsymbol{k},\lambda} \hbar\omega_k r^\dagger_{\boldsymbol{k},\lambda} r_{\boldsymbol{k},\lambda}, \tag{4.1b}$$

$$H_{SR} \equiv \sum_{\boldsymbol{k},\lambda} \hbar\left(\kappa^*_{\boldsymbol{k},\lambda} r^\dagger_{\boldsymbol{k},\lambda}\sigma_- + \kappa_{\boldsymbol{k},\lambda} r_{\boldsymbol{k},\lambda}\sigma_+\right). \tag{4.1c}$$

Note that both the atom-laser and atom-reservoir interactions are in the dipole and rotating wave approximations, and the driving field is now tuned to exact resonance. The scattered field is characterised by the reservoir operators (in the Heisenberg picture)

$$\hat{\boldsymbol{E}}(\boldsymbol{r},t) = \hat{\boldsymbol{E}}^{(+)}(\boldsymbol{r},t) + \hat{\boldsymbol{E}}^{(-)}(\boldsymbol{r},t), \tag{4.2}$$

with

$$\hat{\boldsymbol{E}}^{(+)}(\boldsymbol{r},t) = i\sum_{\boldsymbol{k},\lambda}\sqrt{\frac{\hbar\omega_k}{2\epsilon_0 V}}\,\hat{e}_{\boldsymbol{k},\lambda}\, r_{\boldsymbol{k},\lambda}(t)\, e^{i\boldsymbol{k}\cdot\boldsymbol{r}} \tag{4.3a}$$

$$\hat{\boldsymbol{E}}^{(-)}(\boldsymbol{r},t) = \hat{\boldsymbol{E}}^{(+)}(\boldsymbol{r},t)^\dagger. \tag{4.3b}$$

The Heisenberg equations of motion for the field modes are

$$\dot{r}_{\boldsymbol{k},\lambda} = -i\omega_k r_{\boldsymbol{k},\lambda} - i\kappa^*_{\boldsymbol{k},\lambda}\sigma_- . \tag{4.4}$$

To separate the rapid oscillation due to the free evolution, we introduce the new variables

$$\tilde{r}_{\boldsymbol{k},\lambda} = r_{\boldsymbol{k},\lambda} e^{i\omega_k t}, \tag{4.5a}$$

$$\tilde{\sigma}_- = \sigma_- e^{i\omega_A t}, \tag{4.5b}$$

and integrate (4.4) formally to get

$$\tilde{r}_{\boldsymbol{k},\lambda}(t) = r_{\boldsymbol{k},\lambda}(0) - i\kappa^*_{\boldsymbol{k},\lambda}\int_0^t dt'\tilde{\sigma}_-(t')e^{i(\omega_k-\omega_A)t'} . \tag{4.6}$$

Inserting $r_{\boldsymbol{k},\lambda}(t)$ back into (4.3a) and using the explicit form of $\kappa_{\boldsymbol{k},\lambda}$ from (3.21), the field operator can be expanded in two terms:

$$\hat{\boldsymbol{E}}^{(+)}(\boldsymbol{r},t) = \hat{\boldsymbol{E}}^{(+)}_f(\boldsymbol{r},t) + \hat{\boldsymbol{E}}^{(+)}_a(\boldsymbol{r},t)\,, \tag{4.7}$$

where

$$\hat{\boldsymbol{E}}^{(+)}_f(\boldsymbol{r},t) = i\sum_{\boldsymbol{k},\lambda}\sqrt{\frac{\hbar\omega_k}{2\epsilon_0 V}}\;\hat{e}_{\boldsymbol{k},\lambda}\; r_{\boldsymbol{k},\lambda}(0)\; e^{-i(\omega_k t-\boldsymbol{k}\cdot\boldsymbol{r})}, \tag{4.8}$$

and

$$\hat{\boldsymbol{E}}^{(+)}_a(\boldsymbol{r},t) = i\frac{1}{2\epsilon_0 V}e^{-i\omega_A t}\sum_{\boldsymbol{k},\lambda}\omega_k\hat{e}_{\boldsymbol{k},\lambda}\left(\hat{e}_{\boldsymbol{k},\lambda}\cdot\boldsymbol{\mu}_{12}\right)e^{i\boldsymbol{k}\cdot(\boldsymbol{r}-\boldsymbol{r}_A)} \times\int_0^t dt'\tilde{\sigma}_-(t')e^{i(\omega_k-\omega_A)(t'-t)}. \tag{4.9}$$

The first term in (4.7) describes the free evolution of the reservoir field, while the second describes the field radiated by the atom. The sum and the integral in (4.9) are evaluated to give[1]

$$\hat{\boldsymbol{E}}^{(+)}_a(\boldsymbol{r},t) = -\frac{\omega_A^2}{4\pi\epsilon_0 c^2 r}\left(\boldsymbol{\mu}_{12}\times\hat{r}\right)\times\hat{r}\sigma_-\left(t-r/c\right), \tag{4.10}$$

where $\hat{r} = \boldsymbol{r}/r$. This is identical to the formula for the field radiated by a classical dipole, except that the classical dipole moment has been replaced by the operator $\boldsymbol{\mu}_{12}\sigma_-$.

4.2 Master Equation for Resonance Fluorescence

To derive the master equation for a two-level atom driven by a classical field we follow the same procedure as in the previous chapter. There is one small difference, however. In the derivation of (3.32) we used the Markov approximation to evaluate $g(\boldsymbol{k})$, the density of states of the reservoir, at the resonance frequency ω_A. In reality $g(\boldsymbol{k})$ varies across the natural linewidth of the emitted field, but since this linewidth is very small compared

[1] The sum over $\boldsymbol{k}$ can be converted to an integral which is evaluated using spherical coordinates. For details see [17] pp. 45.

to the frequencies themselves, the variation is negligible. When a classical driving field is introduced we make the same approximation, but we now assume $g(\boldsymbol{k})$ is constant across the frequency range $[\omega_A - \Omega, \omega_A + \Omega]$. This is a more stringent condition but is still easily satisfied at optical frequencies.[2] Consequently, the spontaneous emission rate γ is the same as the free spontaneous emission rate used in chapter 3. The master equation for resonance fluorescence is

$$\begin{aligned}\dot{\rho} = -i\frac{1}{2}\omega_A\left[\sigma_z, \rho\right] + i\frac{\Omega}{2}\left[\sigma_- e^{i\omega_A t} + \sigma_+ e^{-i\omega_A t}, \rho\right] \\ +\frac{\gamma}{2}\left(2\sigma_-\rho\sigma_+ - \sigma_+\sigma_-\rho - \rho\sigma_+\sigma_-\right).\end{aligned} \tag{4.11}$$

4.3 Optical Bloch Equations with Damping

From (4.11) we obtain equations of motion for the expectation values of the atomic operators $\langle\sigma_-\rangle$, $\langle\sigma_+\rangle$, and $\langle\sigma_z\rangle$:

$$\langle\dot{\sigma}_-\rangle = -i\omega_A\langle\sigma_-\rangle - i\frac{\Omega}{2}e^{-i\omega_A t}\langle\sigma_z\rangle - \frac{\gamma}{2}\langle\sigma_-\rangle, \tag{4.12a}$$

$$\langle\dot{\sigma}_+\rangle = i\omega_A\langle\sigma_+\rangle + i\frac{\Omega}{2}e^{i\omega_A t}\langle\sigma_z\rangle - \frac{\gamma}{2}\langle\sigma_+\rangle, \tag{4.12b}$$

$$\langle\dot{\sigma}_z\rangle = i\Omega e^{-i\omega_A t}\langle\sigma_+\rangle - i\Omega e^{i\omega_A t}\langle\sigma_-\rangle - \gamma\left(\langle\sigma_+\rangle + 1\right). \tag{4.12c}$$

These are the optical Bloch equations with radiative damping. The representation in terms of the Bloch vector can still be applied, although the state of the atom is now mixed. We can connect these equations to those seen in Chapter 2 by removing spontaneous emission, setting γ to zero. In that case the state is pure, and the density matrix can be factorised as

$$\rho = |\psi\rangle\langle\psi| = \left(c_1|1\rangle + c_2|2\rangle\right)\left(c_1^*\langle 1| + c_2^*\langle 2|\right). \tag{4.13}$$

The expectation values are

$$\langle\sigma_-\rangle = \rho_{21} = c_1^* c_2, \tag{4.14a}$$

$$\langle\sigma_+\rangle = \rho_{12} = c_1 c_2^*, \tag{4.14b}$$

$$\langle\sigma_z\rangle = \rho_{22} - \rho_{11} = |c_2|^2 - |c_1|^2, \tag{4.14c}$$

so, from equation (2.27), the Bloch vector $\boldsymbol{m}$ is given by

$$\begin{bmatrix} u \\ v \\ w \end{bmatrix} = \begin{bmatrix} \langle\sigma_x\rangle \\ \langle\sigma_y\rangle \\ \langle\sigma_z\rangle \end{bmatrix}, \tag{4.15}$$

where we have used the Pauli pseudo-spin operators defined by equation (2.5). We can generalise the formalism of Section 2.4 by taking (4.15) as the definition of the Bloch vector, allowing for mixed states that do not factorise. Because the state is mixed the length of the Bloch vector is not conserved; $u^2 + v^2 + w^2 \leq 1$. States of the system are now represented by points inside the Bloch sphere, rather than on the surface.

[2] For further details see [17] pp. 46-48

4.4 The Waiting Time Distribution

We can illustrate the quantum properties of the scattered light by looking at the distribution of times between successive spontaneous emissions — the waiting time distribution. For the concept of a photon emission to have physical significance, we envisage surrounding our system by an array of photodetectors. Given that a photon emission is recorded at $t = 0$, what is the probability to record the next photon emission at a later time $t = \tau$? We can answer this question using quantum trajectory theory. The non-Hermitian Hamiltonian for this system follows from the master equation (4.11), and is given by

$$H_{\text{eff}} = \frac{1}{2}\hbar\omega_A\sigma_z - \hbar\frac{\Omega}{2}\left(\sigma_- e^{i\omega_A t} + \sigma_+ e^{-i\omega_A t}\right) - i\hbar\frac{\gamma}{2}\sigma_+\sigma_-. \tag{4.16}$$

If the system is initially in the ground state, the waiting time distribution is the probability density for the system to jump next at time τ, given by

$$W(\tau) = \langle\psi(\tau)|\, J^\dagger J\, |\psi(\tau)\rangle\,, \tag{4.17}$$

where $|\psi\rangle$ is the unnormalised state evolving under (4.16) with initial condition $|\psi(0)\rangle = |1\rangle$.

To calculate $W(\tau)$, we transform into the interaction picture using the free Hamiltonian (2.3). The state in the interaction picture is expanded as

$$\left|\tilde{\psi}(\tau)\right\rangle = \tilde{c}_1(\tau)\,|1\rangle + \tilde{c}_2(\tau)\,|2\rangle \tag{4.18}$$

and inserted into the Schrödinger equation using the interaction Hamiltonian

$$H_{\text{int}} = -\hbar\frac{\Omega}{2}\left(\sigma_- + \sigma_+\right) - i\hbar\frac{\gamma}{2}\sigma_+\sigma_-. \tag{4.19}$$

This leads to the coupled differential equations

$$\frac{d\tilde{c}_1}{d\tau} = \frac{i\Omega}{2}\tilde{c}_2, \tag{4.20a}$$

$$\frac{d\tilde{c}_2}{d\tau} = \frac{i\Omega}{2}\tilde{c}_1 - \frac{\gamma}{2}\tilde{c}_2, \tag{4.20b}$$

with initial conditions $\tilde{c}_1(0) = 1$, $\tilde{c}_2(0) = 0$. These equations are easily solved to give

$$\tilde{c}_1(\tau) = e^{-(\gamma/4)\tau}\left[\cos(\Delta\tau) + \frac{\gamma}{4\Delta}\sin(\Delta\tau)\right], \tag{4.21a}$$

$$\tilde{c}_2(\tau) = i\frac{\Omega}{2\Delta}e^{-(\gamma/4)\tau}\sin(\Delta\tau)\,, \tag{4.21b}$$

where the frequency Δ is given by

$$\Delta = \sqrt{\left(\frac{\Omega}{2}\right)^2 - \left(\frac{\gamma}{4}\right)^2}. \tag{4.22}$$

By casting the solutions in this form we are anticipating that the damping is small, that is

$$\gamma < 2\Omega. \tag{4.23}$$

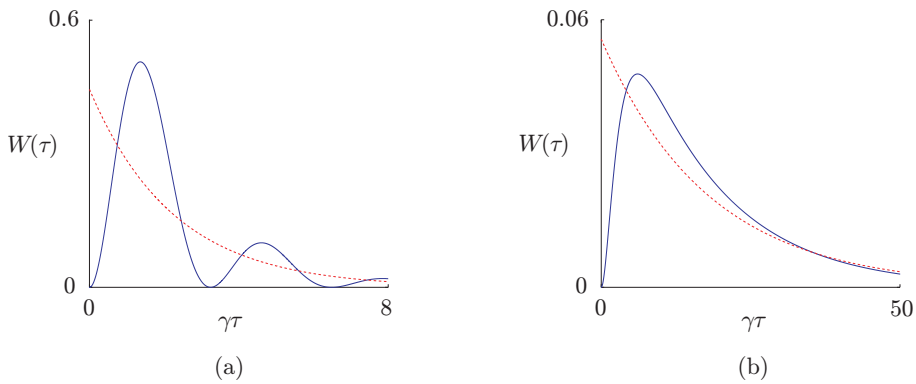

Fig. 4.1: Waiting time distribution for resonance fluorescence (blue line) and the waiting time distribution for a classical source (red line), with parameters (a) $\Omega = 2\gamma$, and (b) $\Omega = \gamma/4$.

This is the 'underdamped' regime, where the solutions are oscillatory. The solutions also hold for larger damping, where Δ becomes imaginary. Using collapse operator (3.47) in equation (4.17), we find

$$W(\tau) = \gamma \left|\tilde{c}_2(\tau)\right|^2 , \tag{4.24}$$

so we arrive at an analytical expression for the waiting time distribution

$$W(\tau) = \gamma \left(\frac{\Omega}{2\Delta}\right)^2 e^{-\frac{\gamma}{2}\tau} \sin^2(\Delta\tau) . \tag{4.25}$$

Some solutions are shown in Fig. 4.1, along with the waiting time distribution for a coherent classical source.[3] The quantum solutions illustrate 'photon antibunching', where the photon emissions are more evenly spaced in time than those from the classical source. This is due to the fact that the atom can only store a single quantum of energy — after the first photon emission it cannot emit again until it is re-excited by the laser field. Photon antibunching for resonance fluorescence was predicted by Carmichael and Walls [20], and later observed experimentally by Kimble *et al.* [21]. The most extensive discussion of it is given in [22].

[3]The classical formula can be found in [17] pp. 64.

Chapter 5

Heating of a Trapped Atom due to Spontaneous Emission

We are now ready to analyse the system that is central to this thesis. We begin by introducing the system, and then use quantum trajectory simulations to see how it evolves. The resulting dynamics are only explained qualitatively; a detailed discussion of the heating and its parameter dependence is the subject of the following two chapters.

5.1 The System

There are three main components in the system:

- **A two-level atom**

  The atom is characterised by the state vector $|\psi\rangle = c_1 |1\rangle + c_2 |2\rangle$, as discussed in Section 2.1. Due to spontaneous emission, however, the general state of the atom is mixed. We treat this using the quantum trajectory formalism developed in Section 3.3.

- **A harmonic trapping potential**

  This is used to confine the atom in space. The source of the potential is not considered in detail. For a neutral atom it could be provided by the Zeeman effect (a magneto-optical trap), or the AC Stark effect (a dipole trap). For an atomic ion, the potential could be provided by an electric field oscillating at radio frequencies (a Paul trap).

- **A coherent electromagnetic field in a standing wave configuration**

  The obvious way to achieve this is by driving the atom with a laser. A single mirror can be used to retro-reflect the laser beam, or the atom can be placed in a cavity. The driving field is exactly at resonance with the atomic transition.

A diagram of the system is shown in Fig. 5.1. The centre of mass motion of the atom is treated classically, and is restricted to one dimension with coordinate x. These are two significant approximations; their validity will be discussed in detail at the end of the chapter.

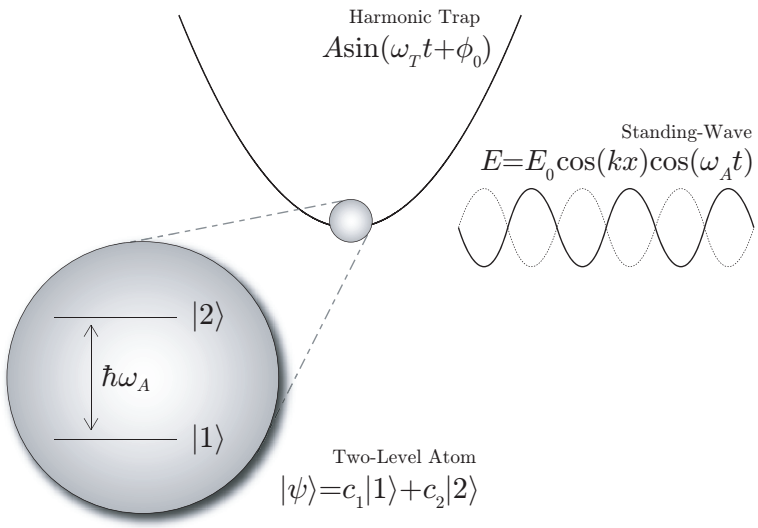

Fig. 5.1: A diagram of the system.

Since the trapping potential is harmonic, the position of the centre of mass is expressed in the form

$$x = A\sin\left(\omega_T t + \phi_0\right), \tag{5.1}$$

where ω_T is the frequency of the trap. In the absence of spontaneous emission A and ϕ_0 are constants, but in general they will vary with time. The driving field is described by the electric field vector

$$\boldsymbol{E}(x,t) = \hat{\boldsymbol{e}}_0 E_0 \cos(kx)\cos(\omega_A t), \tag{5.2}$$

where $k = \omega_A/c = 2\pi/\lambda$. Note that the centre of the trap has been aligned with an antinode of the standing wave.

To calculate the interaction Hamiltonian we follow the same procedure as in Section 2.2, carrying through an additional factor of $\cos(kx)$ to account for the standing wave configuration, and arrive at

$$H_I = \frac{\hbar}{2}\Omega_0 \cos(kx)\left[\sigma_- e^{i\omega_A t} + \sigma_+ e^{-i\omega_A t}\right], \tag{5.3}$$

where Ω_0 is the Rabi frequency defined by equation (2.21). We insert (5.1) into (5.3) and rewrite this as

$$H_I = \frac{\hbar}{2}\Omega(t)\left[\sigma_- e^{i\omega_A t} + \sigma_+ e^{-i\omega_A t}\right], \tag{5.4}$$

where we introduce the time dependent Rabi frequency

$$\Omega(t) = \Omega_0 \cos\left[kA\sin\left(\omega_T t + \phi_0\right)\right]. \tag{5.5}$$

This is how the centre of mass motion is coupled to the internal dynamics of the atom — through the time dependence of the Rabi frequency.

5.1.1 Spontaneous Emission Recoil

When there is a spontaneous emission the atom receives a small momentum kick of magnitude $\hbar k$, equal to the momentum of the emitted photon. To calculate the distribution of emission angles we note that in equation (4.9) for the scattered field, the angular dependence enters via the $(\hat{e}_\lambda \cdot \boldsymbol{\mu}_{12})$ factor. The intensity and emitted photon flux are then proportional to $(\hat{e}_\lambda \cdot \boldsymbol{\mu}_{12})^2$. The polarization of the emitted photons depends on the specific atomic states of our atom; as an example we take linear polarization. We introduce a spherical coordinate system and align the atomic dipole with the z axis, choosing the polarization basis states so that $\hat{e}_{\lambda_1} \cdot \boldsymbol{\mu}_{12} = 0$, as shown in Fig. 5.2. We find

$$(\hat{e}_{\lambda_2} \cdot \boldsymbol{\mu}_{12})^2 \propto \sin^2\theta, \tag{5.6}$$

which, after normalisation, leads to the probability density for the distribution of emission angles

$$p(\theta, \phi) = \frac{3}{8\pi}\sin^2\theta. \tag{5.7}$$

In our one dimensional model we will use the x component of the recoil velocity, which is given by

$$v_x = \frac{h}{m\lambda}\sin\theta\sin\phi, \tag{5.8}$$

where m is the mass of the atom.

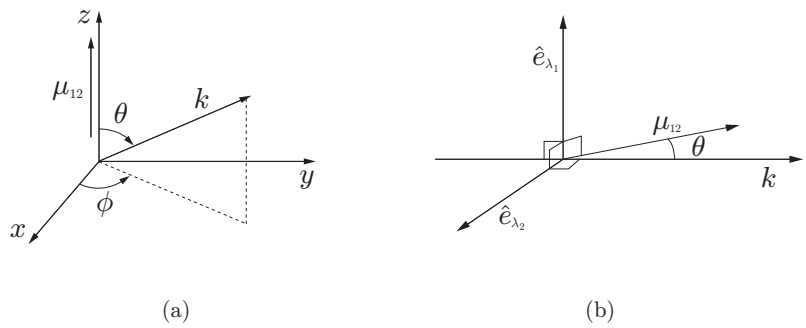

Fig. 5.2: (a) The spherical coordinate system used. (b) The alignment of polarization states.

5.2 Quantum Trajectory Analysis of the System

We are interested in how the atom heats up over time. This can be observed using the formalism of Section 3.3 — we generate trajectories which correspond to the possible outcomes of an experiment where photodetectors record each spontaneous emission. The collapse operator is still given by (3.47), and the effective Hamiltonian of the system is (in the interaction picture)

$$H_{\text{eff}} = -\frac{1}{2}\hbar\Omega(t)\left(\sigma_- + \sigma_+\right) - i\hbar\frac{\gamma}{2}\sigma_+\sigma_-, \tag{5.9}$$

which is identical to (4.16), but with a time dependent Rabi frequency specified by (5.5).

We align the dipole moment of the atom with the z axis, so the distribution of angles at which photons are emitted is given by (5.7). After each collapse the emission angles θ and ϕ are randomly drawn from this distribution. The velocity of the atom is kicked by an amount v_x calculated from (5.8). Trajectories of the system dynamics are generated using the following algorithm:

1. Evaluate the probability to collapse in time Δt
$$\mathrm{P} = \gamma \left\langle \bar{\psi}_n \left| \sigma_+ \sigma_- \right| \bar{\psi}_n \right\rangle \Delta t.$$
2. Draw a uniformly distributed random number between 0 and 1
$$r \sim U(0,1).$$
3. If $r > \mathrm{P}$:
   (a) Collapse the state
$$\left|\psi_{n+1}\right\rangle = \sqrt{\gamma}\sigma_- \left|\bar{\psi}_n\right\rangle.$$
   (b) Draw random variables θ and ϕ and add the corresponding kick velocity
$$v_{n+1} = v_n + \frac{h}{m\lambda}\sin\theta\sin\phi,$$
$$x_{n+1} = x_n.$$
   Otherwise:
   (a) Evolve the atomic state under H_{eff}
$$\frac{d\left|\psi\right\rangle}{dt} = \left[\frac{i\Omega(t)}{2}\left(\sigma_- + \sigma_+\right) - \frac{\gamma}{2}\left(\sigma_+\sigma_-\right)\right]\left|\psi\right\rangle.$$
   (b) Evolve the centre of mass motion according to
$$\frac{d^2x}{dt^2} = -\omega_T^2 x.$$
4. Normalise the new atomic state
$$\left|\bar{\psi}_{n+1}\right\rangle = \frac{\left|\psi_{n+1}\right\rangle}{\sqrt{\left\langle\psi_{n+1}|\psi_{n+1}\right\rangle}}.$$

In Fig. 5.3, two sample trajectories show how the amplitude A evolves. As the atom spontaneously emits, the amplitude fluctuates and tends to increase with time. The simulations were performed for inital conditions $\left|\bar{\psi}(0)\right\rangle = \left|1\right\rangle$, $x(0) = 0$, $v(0) = 0$. However, we will find that the only important initial condition is the initial amplitude

$$A(0) = 0. \tag{5.10}$$

The initial phase of the motion and the inital atomic state have no effect on the system dynamics after many jumps have occured. The evolution between jumps is performed using a second order numerical integration procedure. There is an interesting feature in both graphs: at particular amplitudes the spontaneous emission appears to 'switch off' for a relatively long time. As a result, the atom spends most of its time oscillating at these amplitudes. What is special about them? The rest of the chapter is devoted to a qualitative explanation, while the following chapter explores this phenomenon in more detail.

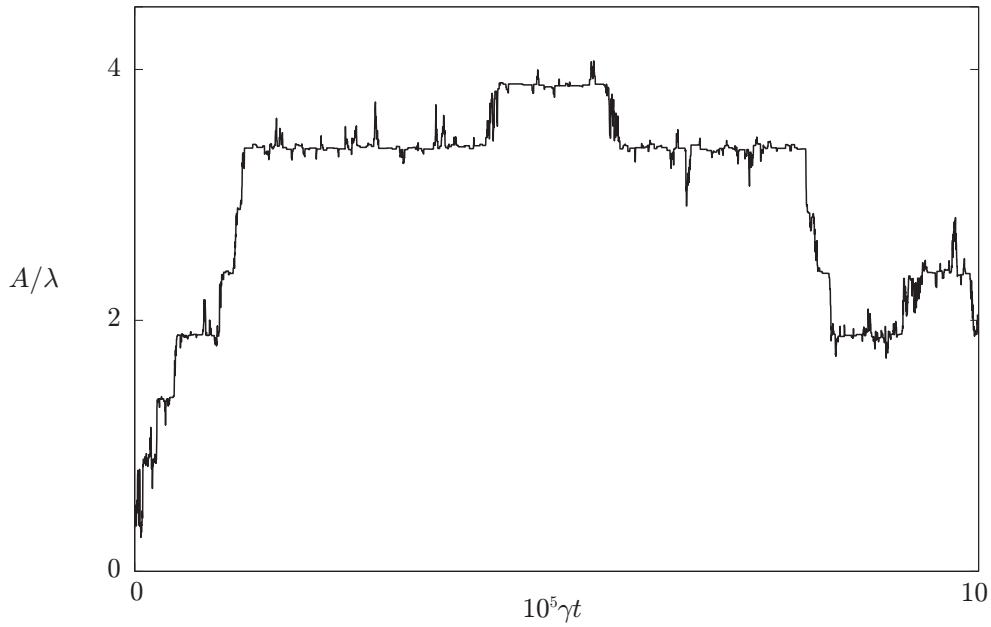

(a)

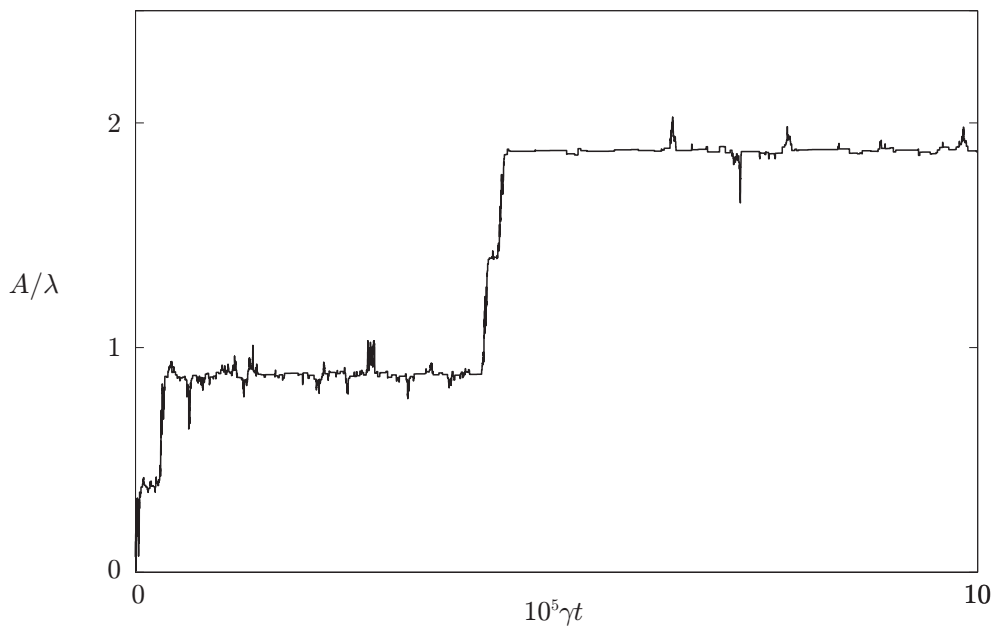

(b)

Fig. 5.3: Sample trajectories of the amplitude evolution. (a) $\Omega_0 = \gamma$, $\omega_T = 2\gamma$. (b) $\Omega_0 = \gamma$, $\omega_T = 5\gamma$. In both graphs the magnitude of the recoil velocity is $v = \gamma\lambda$.

5.3 Metastable Amplitudes

To explain why the atom favours certain amplitudes, we consider the evolution of the system under effective Hamiltonian (5.9). The unnormalised state of the atom (in the interaction picture) is expanded as

$$\left|\tilde{\psi}\right\rangle = \tilde{c}_1 \left|1\right\rangle + \tilde{c}_2 \left|2\right\rangle , \tag{5.11}$$

which leads to the equations

$$\frac{d\tilde{c}_1}{dt} = \frac{i\Omega(t)}{2}\tilde{c}_2, \tag{5.12a}$$

$$\frac{d\tilde{c}_2}{dt} = \frac{i\Omega(t)}{2}\tilde{c}_1 - \frac{\gamma}{2}\tilde{c}_2, \tag{5.12b}$$

where $\Omega(t)$ is specified by (5.5). These are solved numerically, with the initial condition $|\psi(0)\rangle = |1\rangle$. In Fig. 5.4 we plot the quantity

$$|\bar{c}_2(t)|^2 = \frac{|\tilde{c}_2(t)|^2}{|\tilde{c}_1(t)|^2 + |\tilde{c}_2(t)|^2}, \tag{5.13}$$

which is the probability for the atom to be found in the excited state *given a spontaneous emission at $t = 0$ and no further emissions.* In Fig. 5.4 (a) we see something similar to the

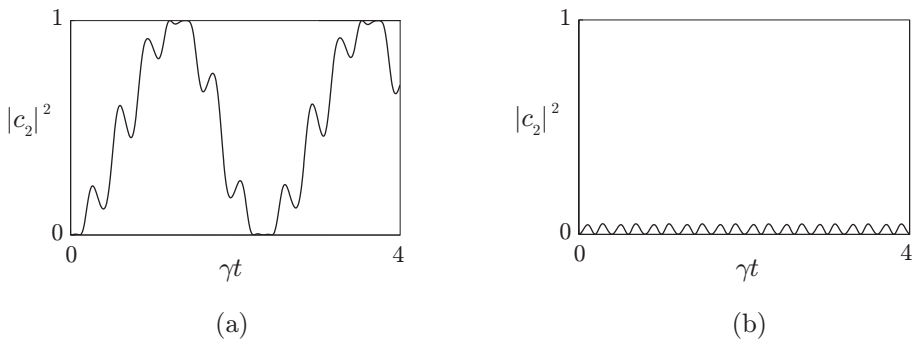

Fig. 5.4: Population inversion of the atom for $\Omega_0 = 10\gamma$, $\omega_T = 10\gamma$. (a) $A/\lambda = 0.3$. (b) $A/\lambda = 0.3827$.

Rabi oscillation studied in Section 2.3. This oscillation has a modulation on top of it, which can be attributed to the motion of the atom through the standing wave. The frequency of oscillation is identified with the cycle average of the time dependent Rabi frequency, given by

$$\langle\Omega(t)\rangle = \frac{\omega_T}{2\pi}\int_0^{\frac{2\pi}{\omega_T}} \Omega(t)\, dt = \Omega_0\, J_0(kA)\,, \tag{5.14}$$

where $J_0(x)$ is a zeroth order Bessel function of the first kind. A review of Bessel functions and their properties is given in Appendix A. In Fig. 5.4 (b) however, we see something quite different. The atom stays down near the ground state, where the probability for a spontaneous emission to occur is very small.

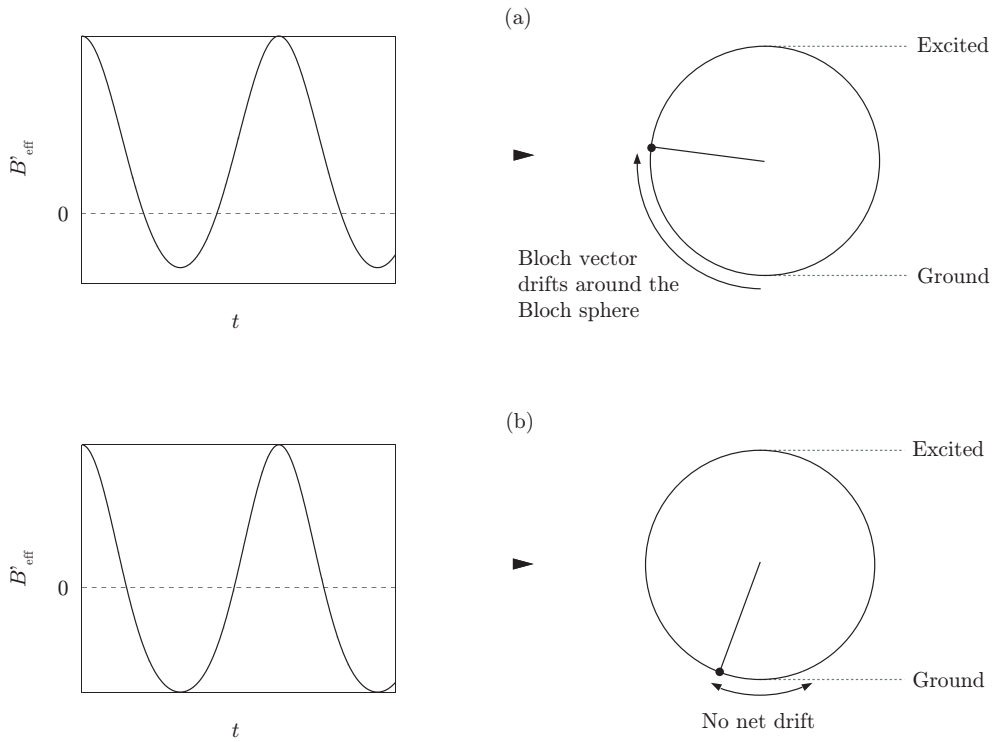

Fig. 5.5: Motion of the Bloch vector. (a) $\langle\Omega(t)\rangle \neq 0$. (b) $\langle\Omega(t)\rangle = 0$.

To explain why this occurs, we consider how the system evolves on the Bloch sphere. The optical Bloch equations for this system follow from the definition (4.15), but we do not consider them in detail. Rather, the Bloch sphere representation is used to develop a qualitative explanation. Spontaneous emission is neglected. From equation (2.32) we infer the effective magnetic field of the system:

$$\boldsymbol{B}'_{\text{eff}} = \begin{bmatrix} 0 \\ \Omega(t) \\ 0 \end{bmatrix}. \tag{5.15}$$

The magnitude of the effective magnetic field oscillates between $-\Omega_0$ and Ω_0. This means the Bloch vector changes direction as it precesses around the Bloch sphere. Since $\boldsymbol{B}'_{\text{eff}}$ always points in the $\pm v$ direction, the Bloch vector is still confined to move within a circle. When the amplitude is just right, the Bloch vector oscillates back and forward but there is no net motion around the Bloch sphere. We call this a "metastable amplitude". At other amplitudes the Bloch vector also oscillates, but during each cycle it travels further in one direction than the other, so there is a net motion in one direction. These two situations are illustrated in Fig. 5.5. To make the Bloch vector oscillate back and forward equally, we require the cycle average of $\boldsymbol{B}'_{\text{eff}}$ to be zero. This seems reasonable, and it will be shown explicitly in the next chapter. Using equation (5.14), we find the metastable amplitudes from the condition

$$J_0\left(\frac{2\pi A}{\lambda}\right) = 0, \tag{5.16}$$

which gives

$$\frac{A}{\lambda} = \{0.3827, 0.8786, 1.3773, 1.8767...\}\,. \tag{5.17}$$

To reiterate the basic idea, we consider an atom moving through a standing wave, as shown in Fig. 5.6. As it moves through a node, the phase of the oscillating electric field flips. The 'response' of the atom (which can, for example, be represented by the motion of the Bloch vector) changes direction. At a metastable amplitude, the response of the atom between two nodes is exactly undone by the response of the atom between the next two nodes. After a spontaneous emission the atom collapses to the ground state, never getting significantly re-excited. The probability for another spontaneous emission to occur becomes very small.

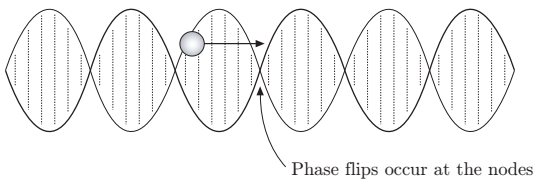

Fig. 5.6: An atom moving through a standing wave.

5.4 Validity of Approximations

Before proceeding further we discuss the validity of the model introduced in this chapter, considering the various approximations made thus far. There are four points to discuss, although the last three are connected.

- **The one dimensional model**
  We have assumed the atom is restricted to motion in one dimension, along a line parallel to the propagation direction of the driving field. In practice an atom will also move in the dimensions orthogonal to this. In fact, since spontaneous emissions occur in all directions, the atom will heat up in the orthogonal dimensions as well. The driving field can be modelled in 3D by

  $$\boldsymbol{E}\left(x,t\right) = \hat{\boldsymbol{e}}_0 E_0 \cos\left(kx\right) e^{-\left(y^2+z^2\right)/r_0^2} \cos\left(\omega_A t\right), \tag{5.18}$$

  which describes a laser beam with waist r_0. Typically this beam waist can be made quite large, of the order of 50μm. On the other hand, a trap can confine the atom in this direction to within 1μm. If the system is configured in this way, the Rabi frequency will not vary significantly as the atom moves back and forward in the radial direction, so a simple one dimensional model should be applicable.

- **The classical centre-of-mass motion**
  We describe the centre of mass by a position variable x, coupling it to the internal state of the atom via the time dependent Rabi frequency. The classical treatment is expected to be valid if there are a large number of quanta in our system — if the atom is high up in the energy levels of the trapping potential. We require

  $$\frac{1}{2} m\omega_T^2 A^2 >> \hbar\omega_T, \tag{5.19}$$

that is, the energy of the centre of mass motion is much larger than the energy associated with the absorption and re-emission of photons. This is the regime we are interested in; where a spontaneous emission is a small perturbation. We begin our simulations at $A = 0$, so strictly speaking the trajectories should be ignored until the system enters this regime — it usually does so very quickly.

- **Spontaneous emission at low energies**

  At high energies, for a momentum kick dp the kinetic energy imparted to the atom is

$$\begin{aligned} \Delta E &= \frac{(p+dp)^2}{2m} - \frac{p^2}{2m}, \\ &= \frac{p\,dp}{2m}, \end{aligned} \tag{5.20}$$

  so as the momentum of the atom decreases, the energy kick from each spontaneous emission will also decrease. At some point the energy kicks become much smaller than the spacing $\hbar\omega_T$ of the energy levels of the trap. Consider an atom cooled to the ground state of the trap: the energy kick from a spontaneous emission is of the order

$$\Delta E = \frac{\hbar^2 k^2}{2m} = \frac{\hbar^2 \omega_A^2}{2mc^2}. \tag{5.21}$$

  For a cesium atom with transition wavelength 852nm this is around 10^{-30}J, while the energy level spacing for a 10MHz trap is around 10^{-27}J. The transition to a higher energy level is far off resonance and is suppressed, so we expect spontaneous emissions to heat the atom more slowly in the low energy regime. Our model will not include this, although it is not significant because we are well outside this regime.

- **The effect of the standing wave on the motion**

  While the atom receives a momentum kick at each spontaneous emission, we have neglected the effect on the centre of mass motion of the absorption of photons from (and their re-emission into) the standing-wave mode. As the atom moves through the standing wave it sees a varying potential, due to the AC Stark effect. It could be incorporated as a classical force (this is not trivial since the potential depends on the internal state of the atom) but we neglect it. Since we are in the regime specified by (5.19), this force is negligible compared to the force of the trap. However, treating the absorption/re-emission processes with this classical force is not the complete picture; they will have a *cumulative* effect on the atomic motion and cause the amplitude to fluctuate in the same way that spontaneous emission does. This cumulative effect may be significant; for example, if we use our model to calculate a final temperature after some period of heating, it will simply give the wrong answer. However, the interesting feature — the presence of metastable amplitudes — should remain. The coherent absorption/re-emission processes will be suppressed along with the spontaneous emission, since they both depend on the population inversion of the atom.

We will find there is a physically accessible region in which all of these approximations hold. The parameters that specify this region will be discussed in the following chapter, while a candidate system is mentioned in Chapter 8.

Additional Notes:

- The magnitude of the recoil velocity used in the simulations described in this chapter is two orders of magnitude larger than the recoil velocity for a heavy atom such as cesium. This is necessary to observe the motion over the scale of a few amplitudes in an achievable computation time. In Chapter 7, a faster method is developed for generating these trajectories, and physical recoil velocities are used. Only the time scale changes; the essential features do not.

- The explanation given in this section only holds when the atom moves fast enough between two nodes that it does not have time to get sufficiently excited — the Bloch vector does not precess very far up the Bloch sphere before it changes direction. This is the case for the graphs in Fig. 5.3. In the opposite case, where the Rabi frequency is much larger than the trap frequency, the Bloch vector can undergo several complete revolutions before it changes direction and the behaviour of the system will be quite different.

Chapter 6

Characterising the Metastable Amplitudes

We have found that in our system the atom is heavily biased towards certain amplitudes. In this chapter we aim to characterise the effect quantitatively, giving a detailed discussion of the parameter dependence. We also make some modifications to the system and see if the metastable amplitudes still exist.

6.1 Waiting Time Distribution

In Section 4.4 we calculated the waiting time distribution for resonance fluorescence. In that case the definition (4.17) was straightforward, but for the system introduced in Chapter 5 we have to be more careful because the Hamiltonian (5.9) has an explicit time dependence. When considering two successive spontaneous emissions, the probability for the second emission to occur depends on where the atom was in the standing wave at the time of the first. Mathematically, we need to specify the intial phase ϕ_0. However, we are interested in the regime where the second photon emission usually occurs long enough after the first so that the initial location of the atom is unimportant. Later in the chapter, when we calculate the average time between spontaneous emissions in this regime, we find there is no dependence on ϕ_0. The two different regimes are depicted in Fig. 6.1, which shows the atom spontaneously emitting as it travels through the standing wave.

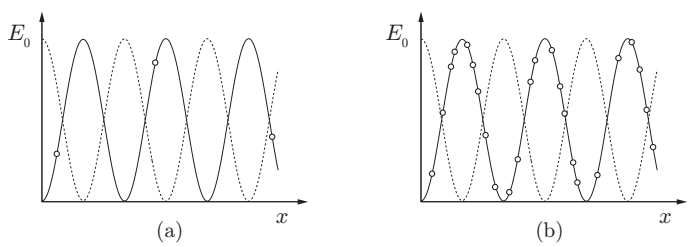

Fig. 6.1: (a) Spontaneous emissions (represented with circles) are sufficiently far apart that the initial phase is unimportant. (b) The time of the next emission will depend on the initial phase.

Proceeding from definition (4.17), we find the waiting time distribution is given by

$$W(\tau) = \gamma \left|\tilde{c}_2(\tau)\right|^2, \tag{6.1}$$

where $\tilde{c}_2(\tau)$ is the solution to (5.12). From (5.12) we find that

$$\begin{aligned} \frac{d}{d\tau}\left\{\left|\tilde{c}_1\right|^2 + \left|\tilde{c}_2\right|^2\right\} &= \frac{d\tilde{c}_1}{d\tau}\tilde{c}_1^* + \frac{d\tilde{c}_1^*}{d\tau}\tilde{c}_1 + \frac{d\tilde{c}_2}{d\tau}\tilde{c}_2^* + \frac{d\tilde{c}_2^*}{d\tau}\tilde{c}_2, \\ &= -\gamma\left|\tilde{c}_2\right|^2, \end{aligned} \tag{6.2}$$

which we can use to show that the distribution is normalised:

$$\begin{aligned} \int_0^\infty W\, d\tau &= \gamma \int_0^\infty \left|\tilde{c}_2\right|^2\, d\tau, \\ &= -\int_0^\infty \frac{d}{d\tau}\left\{\left|\tilde{c}_1\right|^2 + \left|\tilde{c}_2\right|^2\right\} d\tau, \\ &= -\left[\left|\tilde{c}_1\right|^2 + \left|\tilde{c}_2\right|^2\right]_0^\infty, \\ &= 1. \end{aligned} \tag{6.3}$$

Here we have used the fact that $\tilde{c}_1$ and $\tilde{c}_2$ both decay to zero as t tends to infinity. The mean of the waiting time distribution is

$$\langle\tau\rangle = \int_0^\infty \tau W(\tau)\, d\tau. \tag{6.4}$$

Using property (6.2) this can be evaluated as

$$\begin{aligned} \langle\tau\rangle &= -\int_0^\infty \tau \frac{d}{d\tau}\left\{\left|\tilde{c}_1\right|^2 + \left|\tilde{c}_2\right|^2\right\} d\tau \\ &= -\left[\tau\left(\left|\tilde{c}_1\right|^2 + \left|\tilde{c}_2\right|^2\right)\right]_0^\infty + \int_0^\infty \left|\tilde{c}_1\right|^2 + \left|\tilde{c}_2\right|^2\, d\tau \\ &= \int_0^\infty \left|\tilde{c}_1\right|^2 + \left|\tilde{c}_2\right|^2\, d\tau. \end{aligned} \tag{6.5}$$

The mean waiting time $\langle\tau\rangle$ — the average time between spontaneous emissions — can be used to characterise the metastable amplitudes.

6.1.1 Analytic Solution for the Mean Waiting Time

Equations (5.12) can be solved numerically to calculate $\langle\tau\rangle$, but an analytic solution gives more insight into the parameter dependence. Our first step is to make the transformation

$$\tilde{c}_2 \to -i\tilde{c}_2 \tag{6.6}$$

allowing us to rewrite (5.12) as

$$\frac{d\tilde{c}_1}{dt} = -\frac{\Omega(t)}{2}\tilde{c}_2, \tag{6.7a}$$

$$\frac{d\tilde{c}_2}{dt} = \frac{\Omega(t)}{2}\tilde{c}_1 - \frac{\gamma}{2}\tilde{c}_2. \tag{6.7b}$$

Since $\Omega(t)$ and γ are real, we see explicitly that real solutions should exist for $\tilde{c}_1$ and $\tilde{c}_2$. This is related to the fact that the Bloch vector is confined to move within a circle on the Bloch sphere, and is only possible because of the resonance condition $\Delta\omega = 0$. We introduce the complex variable

$$X = \tilde{c}_1 + i\tilde{c}_2, \tag{6.8}$$

with evolution governed by

$$\frac{dX}{dt} = \frac{i\Omega(t)}{2}X - \frac{\gamma}{4}\left(X - X^*\right). \tag{6.9}$$

We decompose X into an amplitude and a phase:

$$X = Me^{i\phi}. \tag{6.10}$$

This yields new equations of motion which are partially decoupled:

$$\frac{dM}{dt} = -\frac{\gamma}{2}M\sin^2\phi, \tag{6.11a}$$

$$\frac{d\phi}{dt} = -\frac{\Omega(t)}{2} - \frac{\gamma}{4}\sin\left(2\phi\right). \tag{6.11b}$$

A solution for M in terms of ϕ can be found by noting that

$$-\frac{\gamma}{2}\sin^2\phi = \frac{1}{M}\frac{dM}{dt} = \frac{d}{dt}\left\{\ln\left(M\right)\right\}, \tag{6.12}$$

which leads to

$$M(t) = M(0)\exp\left\{-\frac{\gamma}{2}\int_0^t \sin^2\left[\phi(t')\right]dt'\right\}. \tag{6.13}$$

In terms of these new variables, the waiting time distribution is

$$W(\tau) = \gamma M^2(\tau)\sin^2[\phi(\tau)], \tag{6.14}$$

and the mean waiting time is

$$\langle\tau\rangle = \int_0^\infty M^2(\tau)\,d\tau. \tag{6.15}$$

From the initial condition $|\psi(0)\rangle = |1\rangle$, we obtain the initial conditions for M and ϕ

$$M(0) = 1, \tag{6.16a}$$

$$\phi(0) = 0. \tag{6.16b}$$

When the mean waiting time is large, we expect the function $M(t)$ to decay slowly. This requires the phase $\phi(t)$ to be small, since the integrand in (6.13) is always positive. From equation (6.11b), we note that the solution for $\phi(t)$ can be small if $\Omega(t)$ has no DC component, so

$$\langle\Omega(t)\rangle = 0. \tag{6.17}$$

Furthermore, when ϕ is small enough we can replace $\sin(2\phi)$ with 2ϕ in equation (6.11b) to obtain

$$\frac{d\phi}{dt} = -\frac{\Omega(t)}{2} - \frac{\gamma}{2}\phi, \tag{6.18}$$

an approximation which turns out to work surprisingly well. We can go ahead and solve this equation for ϕ, starting out by introducing the new variable

$$\psi(t) = \phi(t)e^{\frac{\gamma}{2}t}, \tag{6.19}$$

which evolves according to

$$\frac{d\psi}{dt} = -\frac{\Omega(t)}{2}e^{\frac{\gamma}{2}t}. \tag{6.20}$$

We now insert the function $\Omega(t)$ defined in (5.5) to obtain

$$\psi(t) = -\frac{\Omega_0}{2}\int_0^t e^{\frac{\gamma}{2}t'}\cos\left[\frac{2\pi A}{\lambda}\sin(\omega_T t' + \phi_0)\right]dt'. \tag{6.21}$$

The integral can be evaluated by expanding the cosine in terms of complex exponentials, then using the Bessel function identity

$$e^{ix\sin\theta} = \sum_{n=-\infty}^{\infty} J_n(x)\, e^{in\theta}, \tag{6.22}$$

where $J_n(x)$ is an nth order Bessel function of the first kind. This yields the solution

$$\begin{aligned}\psi(t) &= -\frac{\Omega_0}{4}\sum_{n=-\infty}^{\infty} J_n\left(\frac{2\pi A}{\lambda}\right)\left\{e^{in\phi_0}\left[\frac{e^{\left(\frac{\gamma}{2}+in\omega_T\right)t}-1}{\frac{\gamma}{2}+in\omega_T}\right] + e^{-in\phi_0}\left[\frac{e^{\left(\frac{\gamma}{2}-in\omega_T\right)t}-1}{\frac{\gamma}{2}-in\omega_T}\right]\right\},\\ &= -\frac{\Omega_0}{2}\sum_{n\,\text{even}} J_n\left(\frac{2\pi A}{\lambda}\right)e^{in\phi_0}\left[\frac{e^{\left(\frac{\gamma}{2}+in\omega_T\right)t}-1}{\frac{\gamma}{2}+in\omega_T}\right],\end{aligned} \tag{6.23}$$

where we have used the property $J_{-n}(x) = (-1)^n J_n(x)$. The summation is now over all even values of n. The solution for $\phi(t)$ is then

$$\phi(t) = -\frac{\Omega_0}{2}\sum_{n\,\text{even}} J_n\left(\frac{2\pi A}{\lambda}\right)e^{in\phi_0}\left[\frac{e^{in\omega_T t} - e^{-\frac{\gamma}{2}t}}{\frac{\gamma}{2}+in\omega_T}\right]. \tag{6.24}$$

We have assumed that the mean waiting time is large — we can quantify this by imposing the condition

$$\langle\tau\rangle >> \gamma^{-1}. \tag{6.25}$$

This allows us to neglect the exponential decay term in (6.24) since it is responsible for transient dynamics which have a negligible contribution to the mean if it is much larger than the decay lifetime γ^{-1}. The solution for ϕ becomes

$$\phi(t) = -\frac{\Omega_0}{2}\sum_{n\,\text{even}} J_n\left(\frac{2\pi A}{\lambda}\right)\frac{e^{in(\omega_T t+\phi_0)}}{\frac{\gamma}{2}+in\omega_T}. \tag{6.26}$$

To solve for M we need to integrate $\sin^2\phi$. Again we apply the approximation $\sin\phi \approx \phi$ and find

$$\begin{aligned}\int_0^t \sin^2\left[\phi(t')\right] dt' &\approx \int_0^t \phi^2(t')\, dt' \\ &= \left(\frac{\Omega_0}{2}\right)^2 \sum_{n,m\,\text{even}} J_n J_m \int_0^t \frac{e^{i(n+m)\left(\omega_T t' + \phi_0\right)}}{\left(\frac{\gamma}{2} + in\omega_T\right)\left(\frac{\gamma}{2} + im\omega_T\right)} dt'. \end{aligned} \tag{6.27}$$

For large mean waiting times, when condition (6.25) applies, the only significant contribution to this integral will be the $n+m=0$ term. The other terms oscillate but do not accumulate over time. This is because

$$\int_0^{\frac{2\pi}{\omega}} e^{in\omega t}\, dt = \begin{cases} \frac{2\pi}{\omega} & n = 0 \\ 0 & n \neq 0 \end{cases}. \tag{6.28}$$

Dropping all but the $n+m=0$ term, then integrating, we arrive at

$$\int_0^t \sin^2\left[\phi(t')\right] dt' = \left(\frac{\Omega}{2}\right)^2 \sum_{n\,\text{even}} J_n^2\left(\frac{2\pi A}{\lambda}\right) \frac{t}{\left(\frac{\gamma}{2}\right)^2 + n^2\omega_T^2}, \tag{6.29}$$

which gives the solution for $M(t)$ as a simple exponential decay

$$M(t) = e^{-\beta t}, \tag{6.30}$$

where the decay rate β is

$$\beta = \frac{\gamma}{2}\left(\frac{\Omega_0}{2}\right)^2 \sum_{n\,\text{even}} \frac{J_n^2\left(\frac{2\pi A}{\lambda}\right)}{\left(\frac{\gamma}{2}\right)^2 + n^2\omega_T^2}. \tag{6.31}$$

From equation (6.15), the mean waiting time follows as

$$\begin{aligned}\langle\tau\rangle &= \int_0^\infty e^{-2\beta\tau}\, d\tau, \\ &= \frac{1}{2\beta}, \\ &= \frac{4}{\gamma\Omega_0^2}\left\{\sum_{n\,\text{even}} \frac{J_n^2\left(\frac{2\pi A}{\lambda}\right)}{\left(\frac{\gamma}{2}\right)^2 + n^2\omega_T^2}\right\}^{-1}. \end{aligned} \tag{6.32}$$

This solution is consistent with the definition of the metastable amplitudes in (5.16). For most amplitudes the dominant term in the sum in (6.32) is the $n = 0$ term, but when condition (5.16) holds this vanishes. The mean waiting time is proportional to the inverse of this sum, so it increases. We also note that the location of the atom at $t = 0$, represented by phase ϕ_0, is not present in the solution. It drops out when the oscillating terms are neglected in the integral in (6.27).

In Fig. 6.2 (a) we compare the analytic solution (6.32) to the solution found by numerically integrating (5.12). They are in very good agreement for mean waiting times larger than about $10\gamma^{-1}$. In Fig. 6.2 (b) we see how many terms must be included in the sum in (6.32). For amplitudes around one wavelength, only the first few terms in the sum need to be calculated, but as the amplitude increases the series converges more slowly, so more terms must be included.

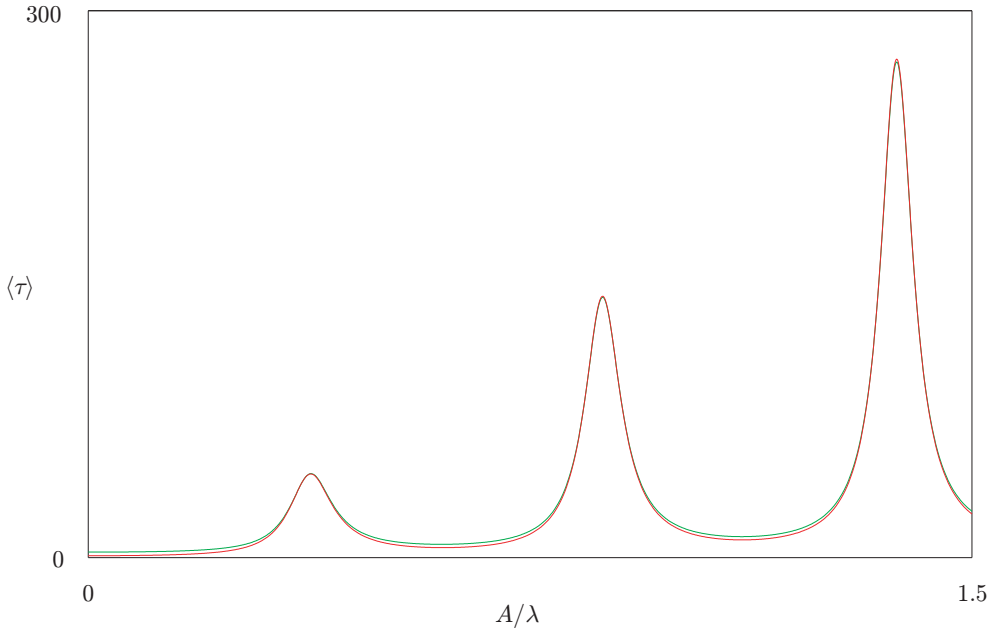

(a)

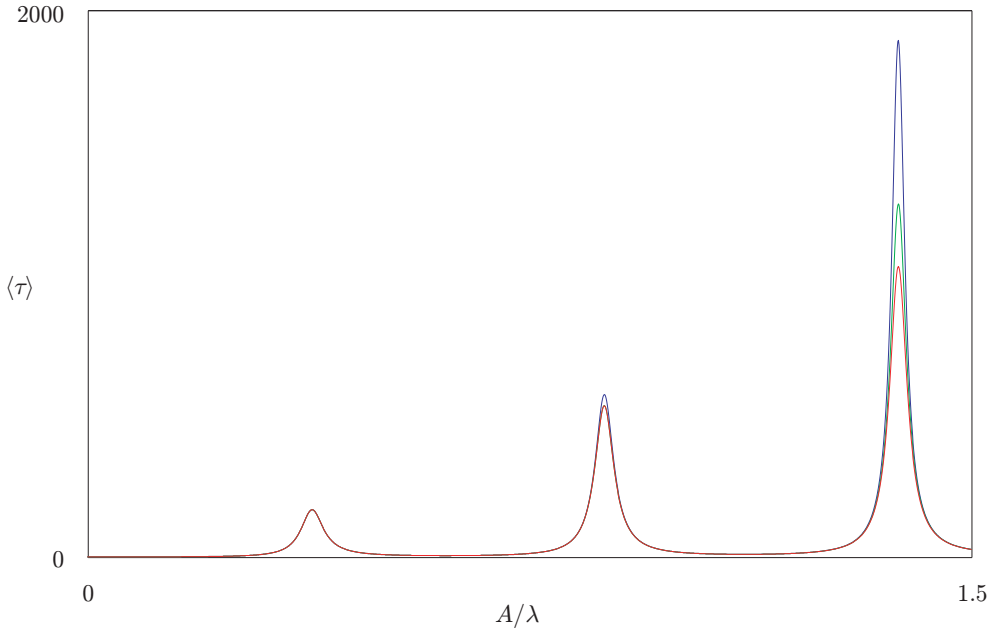

(b)

Fig. 6.2: (a) Comparison of mean waiting times calculated with the analytical solution (red line) and the numerical solution (green line). Parameters used are $\Omega_0 = \gamma$, $\omega_T = \gamma$, and terms in the analytic solution are evaluated up to $|n| = 20$. (b) Analytic solution for parameters $\Omega_0 = \gamma$, $\omega_T = 2\gamma$, including terms up to $|n| = 4$ (blue line), $|n| = 6$ (green line), and $|n| = 100$ (red line).

6.1.2 Parameter Dependence

From the graphs we have seen so far, we find that around the metastable amplitudes the mean waiting time increases, in some cases by several orders of magnitude. There are three parameters that affect the amplitude dependence of the the mean waiting time:

- **The maximum Rabi frequency Ω_0**

  In an experimental setup this will be controlled by varying the output power of the laser that produces the driving field, but it also depends on the dipole coupling strength of the atom-field interaction.

- **The trap frequency ω_T**

  How this is controlled depends on the particular type of trap; in a dipole trap, for example, it will depend on the output power and wavelength of the trapping laser, and the mass of the atom.

- **The spontaneous emission parameter γ**

  This is set by the particular choice of atomic transition, since γ is the probability per unit time for the atom to decay from the excited state to the ground state in free space.

Multiplying these three parameters by a constant just changes the timescale of the evolution, so we fix γ and measure Ω_0 and ω_T with respect to it.

From the analytic solution (6.32) we see immediately that Ω_0 only appears as a constant scaling factor. In the regime where the mean waiting time is large, it is proportional to Ω_0^{-2}. The dependence on ω_T is more complicated. The $n = 0$ term in (6.32) is independent of ω_T, and when ω_T increases the $n \neq 0$ terms get smaller, so the $n = 0$ term becomes more dominant. Thus, when the trap frequency is increased we expect the peaks to get sharper, and this is indeed what occurs. Fig. 6.3 illustrates the parameter dependence. In Fig. 6.3 (a) to Fig. 6.3 (d) the approximation of large mean waiting times holds; Ω_0 only changes the vertical scale, and when ω_T is increased the peaks become narrow and tall. The approximation fails at low trap frequencies and/or high maximum Rabi frequencies. Numerical solutions for the mean waiting time in this regime are shown in Fig. 6.3 (e) and Fig. 6.3 (f). There is a lot of interesting structure here, but explaining it is a project for future research; we only note that the mean waiting time varies less dramatically with amplitude.

The metastable amplitudes should be more prominent for a high trap frequency and a low maximum Rabi frequency. Of course, if the peaks get too sharp the atom may never hit exactly the right amplitude as it gets kicked around, but for realistic kick velocities and trap frequencies this will never occur as the change in amplitude from a single spontaneous emission is exceedingly small.

6.2 Extensions of the Model

When discovering an effect like this in a simplified theoretical model, a question immediately arises: will the effect be observable in an experiment? With this question in mind, we now make two extensions to the model which may be of significance in a practical experimental setup.

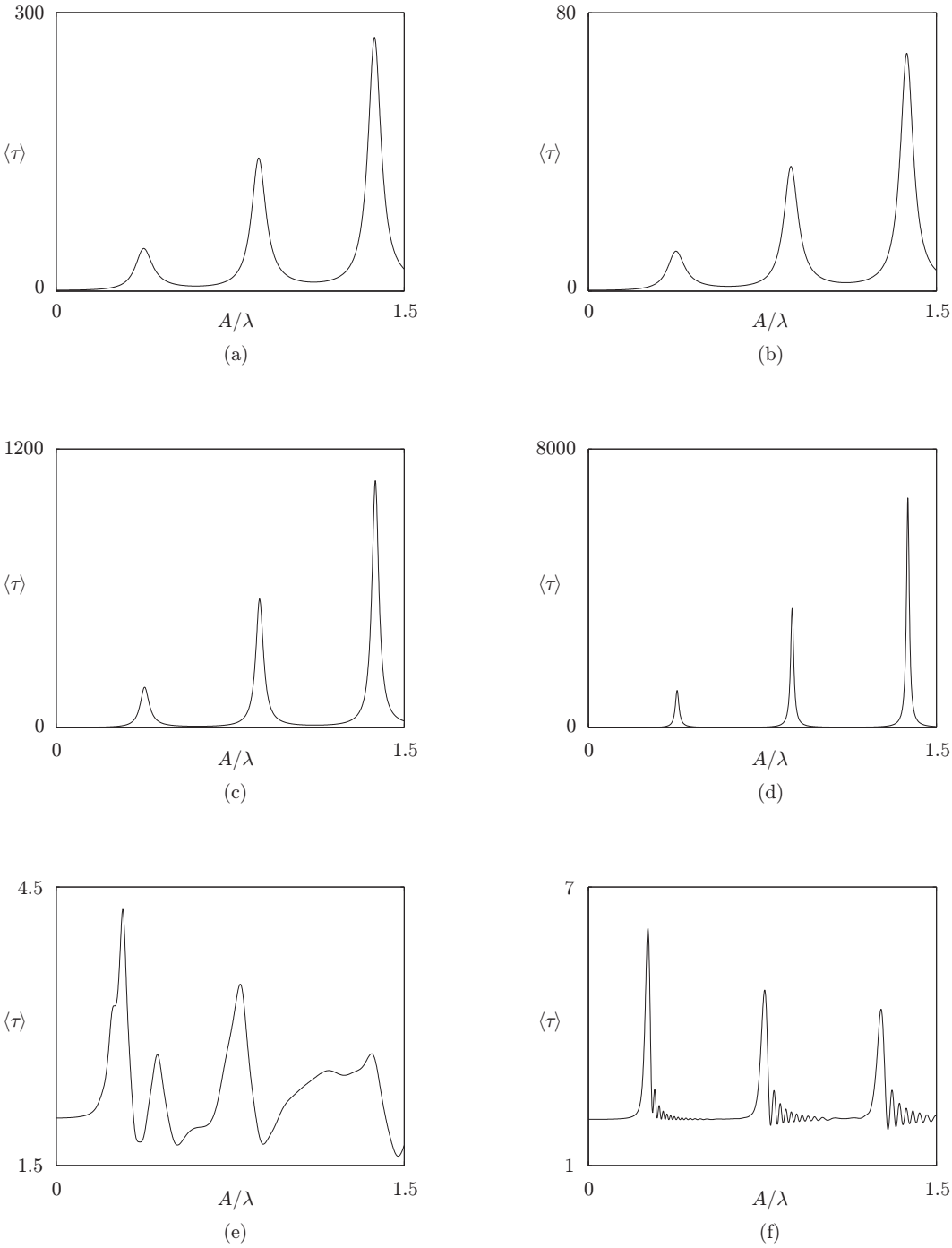

Fig. 6.3: Amplitude dependence of the mean waiting time. (a) $\Omega_0 = \gamma$, $\omega_T = \gamma$. (b) $\Omega_0 = 2\gamma$, $\omega_T = \gamma$. (c) $\Omega_0 = \gamma$, $\omega_T = 2\gamma$. (d) $\Omega_0 = \gamma$, $\omega_T = 5\gamma$. (e) $\Omega_0 = 6\gamma$, $\omega_T = 0.5\gamma$. (f) $\Omega_0 = 10\gamma$, $\omega_T = 0.1\gamma$.

6.2.1 Phase Offset

When specifying the driving field with equation (5.2) we aligned the centre of the trapping potential with an antinode of the standing wave. If the trap centre is offset by a phase ξ, the driving field is

$$\boldsymbol{E}(x,t) = \hat{\boldsymbol{e}}_0 E_0 \cos(kx+\xi)\cos(\omega_A t)\,, \tag{6.33}$$

leading to a time dependent Rabi frequency

$$\Omega(t) = \Omega_0 \cos\left[kA\sin(\omega_T t+\phi_0)+\xi\right]. \tag{6.34}$$

This situation is more realistic; it is likely that there will be some misalignment in a practical setup. Again we can pursue an analytic solution for the mean waiting time, solving (5.12) with $\Omega(t)$ specified by (6.34). We follow the same procedure up to (6.20), then insert (6.34) to obtain

$$\psi(t) = -\frac{\Omega_0}{2}\int_0^t e^{\frac{\gamma}{2}t'}\cos\left[\frac{2\pi A}{\lambda}\sin(\omega_T t'+\phi_0)+\xi\right]dt'. \tag{6.35}$$

Expanding the cosine in terms of Bessel functions, we find the solution for $\psi(t)$ is

$$\psi(t) = -\frac{\Omega_0}{4}\sum_{n=-\infty}^{\infty} J_n\left(\frac{2\pi A}{\lambda}\right)\left\{e^{i(n\phi_0+\xi)}\left[\frac{e^{\left(\frac{\gamma}{2}+in\omega_T\right)t}-1}{\frac{\gamma}{2}+in\omega_T}\right]\right.$$
$$\left.+e^{-i(n\phi_0+\xi)}\left[\frac{e^{\left(\frac{\gamma}{2}-in\omega_T\right)t}-1}{\frac{\gamma}{2}-in\omega_T}\right]\right\}. \tag{6.36}$$

This gives the solution for $\phi(t)$, which we drop the decay terms from to obtain

$$\phi(t) = -\frac{\Omega_0}{4}\sum_{n=-\infty}^{\infty} J_n\left(\frac{2\pi A}{\lambda}\right)\left\{\frac{e^{i(n\omega_T t+n\phi_0+\xi)}}{\frac{\gamma}{2}+in\omega_T}+\frac{e^{-i(n\omega_T t+n\phi_0+\xi)}}{\frac{\gamma}{2}-in\omega_T}\right\}. \tag{6.37}$$

Squaring this and integrating, excluding the oscillatory terms, we find that the solution for $M(t)$ is still an exponential decay, with

$$\beta = \frac{\gamma}{4}\left(\frac{\Omega_0}{2}\right)^2\sum_{n=-\infty}^{\infty}\frac{J_n^2\left(\frac{2\pi A}{\lambda}\right)\left[1+(-1)^n\cos(2\xi)\right]}{\left(\frac{\gamma}{2}\right)^2+n^2\omega_T^2}. \tag{6.38}$$

The mean waiting time follows:

$$\langle\tau\rangle = \frac{8}{\gamma\Omega_0^2}\left\{\sum_{n=-\infty}^{\infty}\frac{J_n^2\left(\frac{2\pi A}{\lambda}\right)\left[1+(-1)^n\cos(2\xi)\right]}{\left(\frac{\gamma}{2}\right)^2+n^2\omega_T^2}\right\}^{-1}. \tag{6.39}$$

When $\xi = 0$, the odd terms drop out of the sum and this reduces to (6.32). In Fig. 6.4 we see that as ξ is increased from zero, the height of the peaks decreases. For small phase offsets the peaks are still located by condition (5.16). For large phase offsets the peaks shift, as the odd terms begin to contribute to the sum and the $n = 0$ term is no longer dominant. As ξ approaches the maximum offset of 90° a peak occurs around $A = 0$; this is because the atom stays near a node of the standing wave. The important point to note is that the metastable amplitudes are still present; they are not destroyed by the asymmetry introduced with the phase offset.

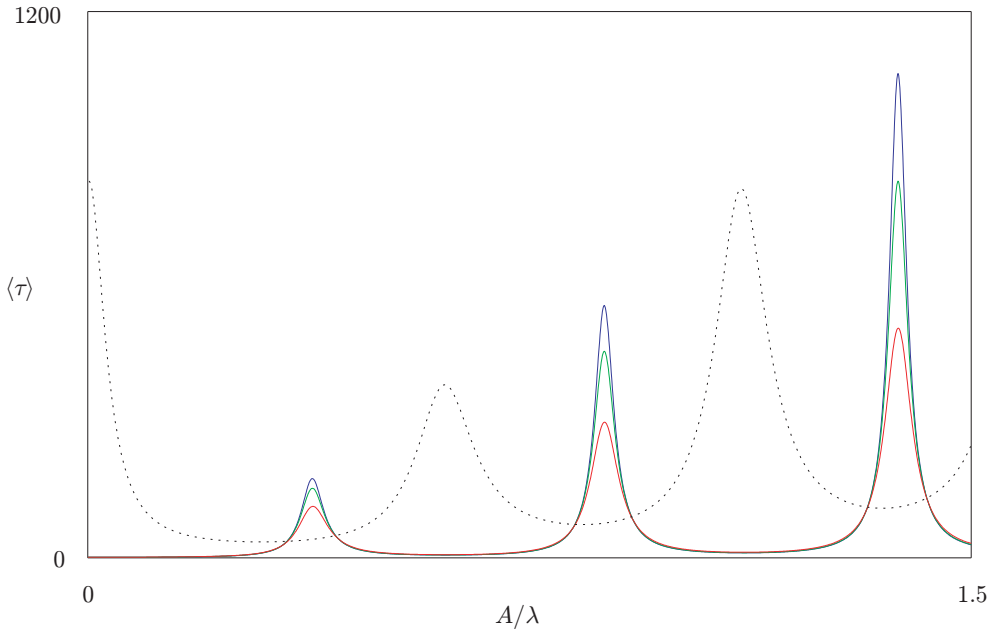

Fig. 6.4: Mean waiting time with a phase offset $\xi = 0$ (blue line), $\xi = 10°$ (green line), $\xi = 20°$ (red line), and $\xi = 85°$ (dashed line), for parameters $\Omega_0 = \gamma$, $\omega_T = 2\gamma$.

6.2.2 Detuning

In a practical experimental setup there may be a detuning between the driving field and the atomic transition. If the driving field is specified as

$$\boldsymbol{E}(x,t) = \hat{\boldsymbol{e}}_0 E_0 \cos(kx) \cos(\omega t), \tag{6.40}$$

the full Hamiltonian of the system is

$$H = \frac{1}{2}\hbar\omega_A + \frac{1}{2}\hbar\Omega(t)\left(\sigma_- e^{i\omega t} + \sigma_+ e^{-i\omega t}\right), \tag{6.41}$$

where $\Omega(t)$ is still given by (5.5). Transforming into the interaction picture using the free Hamiltonian (2.3), and making use of the Baker-Hausdorff formula (2.18), we find

$$\tilde{H}_I = -\frac{1}{2}\hbar\Delta\omega\sigma_z - \frac{1}{2}\hbar\Omega(t)\left(\sigma_+ + \sigma_-\right), \tag{6.42}$$

where $\Delta\omega = \omega - \omega_A$. The effective Hamiltonian for evolution between jumps is then

$$H_{\text{eff}} = -\frac{1}{2}\hbar\Delta\omega\sigma_z - \frac{1}{2}\hbar\Omega(t)\left(\sigma_- + \sigma_+\right) - i\hbar\frac{\gamma}{2}\sigma_+\sigma_-. \tag{6.43}$$

Expanding the state as in (5.11), we obtain the coupled differential equations

$$\frac{d\tilde{c}_1}{dt} = -\frac{i\Delta\omega}{2}\tilde{c}_1 + \frac{i\Omega(t)}{2}\tilde{c}_2, \tag{6.44a}$$

$$\frac{d\tilde{c}_2}{dt} = \frac{i\Delta\omega}{2}\tilde{c}_2 + \frac{i\Omega(t)}{2}\tilde{c}_1 - \frac{\gamma}{2}\tilde{c}_2. \tag{6.44b}$$

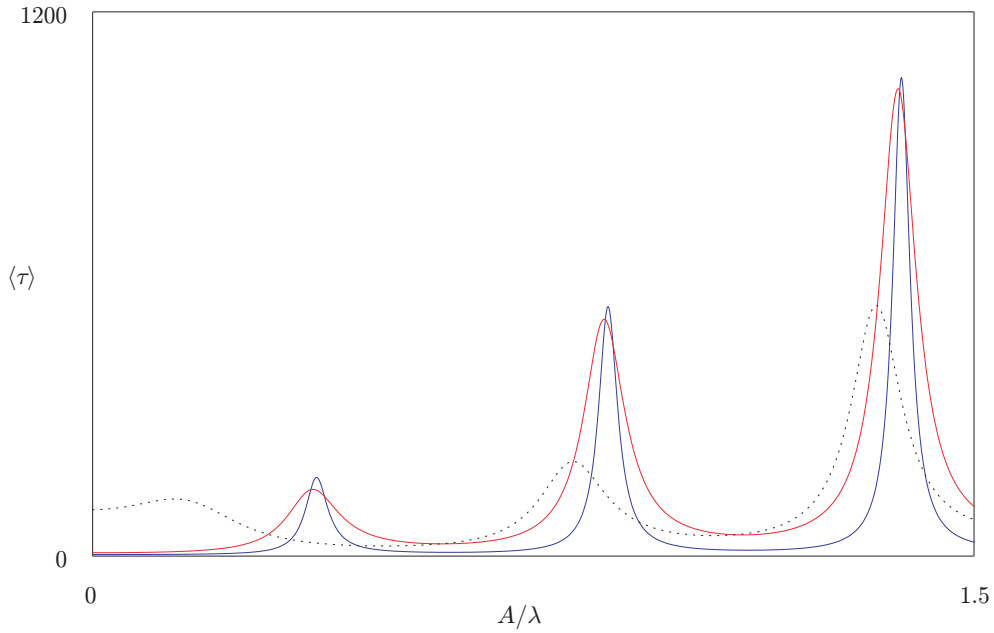

Fig. 6.5: Mean waiting time with a detuning $\Delta\omega = 0$ (blue line), $\Delta\omega = \gamma$ (red line), and $\Delta\omega = 5\gamma$ (dashed line).

With the introduction of a detuning, the dynamics of the system become more complicated. The Bloch vector is no longer confined to move within a circle and we cannot look for real solutions to the equations as in Section 6.1.1. The equations are solved numerically and the mean waiting time is calculated. In Fig. 6.5 we see the result: for small detunings the metastable ampitudes are still present. As the detuning is increased from zero, the peaks get lower and shift to the left. For large detunings ($\Delta\omega >> \gamma$) the metastable amplitudes disappear.

Chapter 7

A Diffusion Model of the Heating Process

So far, we have investigated the heating of a trapped atom by watching the amplitude of oscillation evolve stochastically. The trajectories that are generated will vary from one run to the next; to quantify this variation, we need to calculate averages over many different runs. This is difficult using the quantum trajectory procedure outlined in Section 5.3, because a single trajectory takes a considerable time to generate — around an hour or two on a good desktop PC. The probability to spontaneously emit over a single timestep must be very small, so generating trajectories with thousands of spontaneous emissions involves a lot of calculation. Furthermore, if we wish to see significant heating using physical values for the recoil velocities, we need to evolve out to times where *millions* of spontaneous emissions have occured. In this chapter we model the heating of the atom as a diffusion process where many spontaneous emissions occur over a single timestep.

7.1 Diffusion as the Limit of a Random Walk

A diffusion process can be arrived at as the limit of a random walk when the stepsize goes to zero and the jump rate goes to infinity. We begin by reviewing this procedure for a simple random walk, following closely the treatment of Gardiner [23].

7.1.1 The Wiener Process

The Wiener process is a stochastic process describing the evolution of a random variable $W(t)$. It can be defined as the solution of the one dimensional Fokker-Planck equation with zero drift and unit diffusion

$$\frac{\partial}{\partial t} p\left(w, t|w_0, t_0\right) = \frac{1}{2}\frac{\partial^2}{\partial w^2} p\left(w, t|w_0, t_0\right), \tag{7.1}$$

with the initial condition

$$p\left(w, t_0|w_0, t_0\right) = \delta\left(w - w_0\right). \tag{7.2}$$

We can solve this equation with the characteristic function

$$\phi\left(s,t\right)=\int p\left(w,t|w_0,t_0\right)\,e^{isw}\,dw, \tag{7.3}$$

which satisfies the equation

$$\frac{\partial\phi}{\partial t}=-\frac{1}{2}s^2\phi. \tag{7.4}$$

This has the solution

$$\phi(s,t)=\phi(s,t_0)\,e^{-\frac{1}{2}s^2(t-t_0)}, \tag{7.5}$$

which, after applying the initial condition (7.2), becomes

$$\phi(s,t)=e^{isw_0-\frac{1}{2}s^2(t-t_0)}. \tag{7.6}$$

We find the solution to (7.1) by taking the inverse Fourier transform, obtaining

$$p\left(w,t_0|w_0,t_0\right)=\frac{1}{\sqrt{2\pi\left(t-t_0\right)}}\,e^{-(w-w_0)^2/2(t-t_0)}. \tag{7.7}$$

This is a Gaussian probability distribution with mean w_0 and variance $(t-t_0)$. The Wiener process can be simulated by breaking an interval into discrete timesteps, after each timestep Δt adding the increment

$$\Delta W=\zeta\sqrt{\Delta t} \tag{7.8}$$

where ζ is a random number drawn from a normal distribution with zero mean and unit variance. In the limit that Δt tends to dt, ΔW tends to the Wiener increment dW.

7.1.2 The Random Walk in One Dimension

Consider a person moving along a line, making a jump of size l backwards or forwards with constant probability per unit time d. Their position can take on any value nl, where n is an integer. The transition probability per unit time is

$$W\left(n+1|n,t\right)=W\left(n-1|n,t\right)=d; \tag{7.9}$$

otherwise $W\left(n|m,t\right)=0$. The master equation for the probability to be at position nl given a starting point of $n'l$ is

$$\frac{\partial}{\partial t}P\left(n,t|n',t'\right)=d\left[P\left(n+1,t|n',t'\right)+P\left(n-1,t|n',t'\right)-2P\left(n,t|n',t'\right)\right], \tag{7.10}$$

which is easily solved via the characteristic function

$$G\left(s,t\right)=\sum_n P\left(n,t|n',t'\right)\,e^{ins}, \tag{7.11}$$

so the master equation gives

$$\frac{\partial}{\partial t}G\left(s,t\right)=d\left(e^{is}+e^{-is}-2\right)G\left(s,t\right). \tag{7.12}$$

We take the initial condition $n' = 0$ at $t = 0$, which requires

$$G(s,0) = 1, \tag{7.13}$$

so the solution for the characteristic function is

$$G(s,t) = \exp\left[\left(e^{is} + e^{-is} - 2\right) td\right]. \tag{7.14}$$

The probability distribution $P(n,t|n',t')$ can be found by expanding $G(s,t)$ in powers of e^{is}, but we are interested in the characteristic function itself. We move to a continous state space, with distance travelled $x = nl$. The characteristic function for the distribution of x is

$$\phi(s,t) = G(ls,t) = \exp\left[\left(e^{ils} + e^{-ils} - 2\right) td\right]. \tag{7.15}$$

If we take the limit

$$\begin{aligned} l &\longrightarrow 0, \\ d &\longrightarrow \infty, \end{aligned}$$

so that

$$\left(e^{ils} + e^{-ils} - 2\right) \longrightarrow -l^2 s^2, \tag{7.16}$$

the characteristic function becomes

$$\phi(s,t) \longrightarrow e^{-\frac{1}{2}s^2 Dt}, \tag{7.17}$$

where

$$D = 2 \lim_{\substack{l \to 0 \\ d \to \infty}} \left(l^2 d\right). \tag{7.18}$$

This is the characteristic function for the Gaussian probability distribution

$$p(x,t|0,0) = \frac{1}{\sqrt{2\pi Dt}} e^{-x^2/2Dt}, \tag{7.19}$$

which describes a Wiener process where the time is rescaled by a factor of D (the variance is now Dt). Thus we see that, for small stepsizes, a random walk with stepsize l and jump rate d can be approximated by a Wiener process with diffusion coefficient D.

7.2 The Diffusion Limit in Our System

To approximate our heating process as a diffusion process, we must make some simplifications to the model. To generate the trajectories in Section 5.3, we chose a random emission direction each time a collapse occured, then kicked the atom accordingly. We simplify this, introducing a mean square recoil velocity so that we have a constant stepsize. This should not change any of the features of the heating process that we are interested in. The mean square average of the x component of the recoil velocity is

$$\left\langle v_x^2 \right\rangle = \int P_{v_x}(\theta,\phi)\, v_x(\theta,\phi)\, d\Omega, \tag{7.20}$$

where $P_{v_x}(\theta,\phi)\,d\Omega$ is the probability of getting a spontaneous emission through solid angle $d\Omega$ around point (θ,ϕ). Using the co-ordinate system of Fig. 5.2 (a) and equations (5.7) and (5.8), we find

$$\begin{aligned}\langle v_x^2\rangle &= \frac{3}{8\pi}\left(\frac{h}{m\lambda}\right)^2\int_0^{2\pi}\sin^2\phi\,d\phi\int_0^{\pi}\sin^5\theta\,d\theta,\\ &= \frac{2}{5}\left(\frac{h}{m\lambda}\right)^2.\end{aligned}\tag{7.21}$$

Note that we are still considering an atom with its dipole moment aligned in the z direction, just like in Section 5.2. If the dipole is aligned in the direction of motion x, the field does not couple to the atom at all and we get the trivial solution — no excitation and no spontaneous emission. Excepting this case, the alignment of the atomic dipole is not an important consideration as the average kick velocity doesn't affect the qualitative properties of the heating process.

The change in amplitude $(\Delta A)_1$ from a small velocity kick Δv_x follows from the SHM equation

$$A=\sqrt{x^2+\left(\frac{v_x}{\omega_T}\right)^2},\tag{7.22}$$

so we obtain

$$(\Delta A)_1\approx\left(\frac{\partial A}{\partial v_x}\right)\Delta v_x=\frac{v_x}{w_T^2 A}\,\Delta v_x.\tag{7.23}$$

This implies the amplitude kick is zero (to first order) if the atom spontaneously emits while at a turning point in the trap. From (7.23) and (5.1) it follows that

$$(\Delta A)_1^2=\frac{\cos^2(\omega_T t+\phi_0)}{\omega_T^2}\,(\Delta v_x)^2\,.\tag{7.24}$$

During the evolution ϕ_0 will also evolve stochastically, as it gets kicked with each spontaneous emission as well as the amplitude. We are going to take the limit where the jump size tends to zero and the jump rate tends to infinity. In this limit it is acceptable to replace the cosine with its cycle average, ignoring the stochastic evolution of ϕ_0. The jumps will occur at all points in the cycle, but A and ϕ_0 will not change significantly over a single cycle, as we take the limit in such a way that the total heating rate is the same as in our previous model. We obtain

$$\begin{aligned}(\Delta A)_1^2 &= \frac{1}{2\,\omega_T^2}\,(\Delta v_x)^2\,,\\ &= \frac{1}{2\,\omega_T^2}\,\langle v_x^2\rangle\,,\\ &= \frac{1}{5\,\omega_T^2}\left(\frac{h}{m\lambda}\right)^2.\end{aligned}\tag{7.25}$$

Another ingredient of the diffusion model is the probability per unit time for a spontaneous emission to occur (the jump rate). In Chapter 6 we developed analytical and numerical

solutions for the average time between spontaneous emissions, the jump rate d is simply its inverse:

$$d = \frac{1}{\langle \tau \rangle}. \tag{7.26}$$

Note that this is where the amplitude dependence enters the model, as the mean waiting time varies significantly with amplitude.

For a given amplitude, we consider an interval Δt which is significantly larger than the mean waiting time. However, it is still small enough so that the jump rate d is approximately constant. Then, over this interval, the jump process can be approximated by a diffusion process as in Section 7.1.2. Using equation (7.18) we obtain the diffusion coefficient

$$D = \frac{2}{5\,\omega_T^2\,\langle \tau \rangle} \left(\frac{h}{m\lambda} \right)^2. \tag{7.27}$$

Over the interval Δt, the stochastic evolution of the system is approximated as a Wiener process. The change in amplitude over this interval is

$$\begin{aligned} \Delta A &= \sqrt{D(A)}\,\Delta W, \\ &= \sqrt{D(A)\,\Delta t}\,\zeta. \end{aligned} \tag{7.28}$$

To evaluate $D(A)$ at a given amplitude it is possible to use either the analytical or numerical solutions for the mean waiting time. We use the analytical solution, but switch to the numerical solution for amplitudes where the analytical solution predicts that the mean waiting time will be less than $100\gamma^{-1}$. This results in a fast program, and avoids the numerical inaccuracies which can occur around the peaks when the mean waiting time is very large. From a stored vector of $D(A_i)$ values, we generate trajectories using a linear interpolation method to determine the diffusion coefficient at each amplitude we arrive at. Starting from $A = 0$ at $t = 0$, the procedure is as follows:

1. Given an amplitude A_t at time t, calculate the diffusion coefficient

$$D\left(A_t\right) = D\left(A_j\right) + \left(A_t - A_j\right) \frac{D\left(A_{j+1}\right) - D\left(A_j\right)}{A_{j+1} - A_j},$$

   where

$$A_j < A_t < A_{j+1}.$$

2. Draw a normally distributed random number with zero mean and unit variance

$$\zeta \sim N(0, 1).$$

3. Calculate the new amplitude

$$A_{t+\Delta t} = A_t + \sqrt{D\left(A_t\right)\Delta t}\,\zeta. \tag{7.29}$$

The timestep Δt must be carefully chosen. While evolving, we check to see that after every step the diffusion coefficient does not change by more than a few percent of its local average. The local average is the average value of the diffusion coefficient over an amplitude range of half a wavelength, as illustrated in Fig. 7.1.

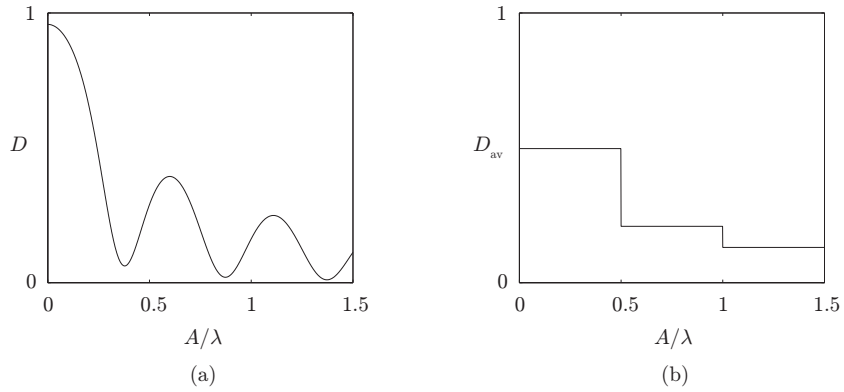

Fig. 7.1: Diffusion coefficient (in arbitray units) for $\Omega_0 = \gamma$, $\omega_T = \gamma$. (a) Full amplitude dependence. (b) Averages used to check that the timestep is not too large.

7.3 Results

In this section we view the results of the diffusion model using parameters that should be achievable in an experimental setup. We generate some trajectories to show the stochastic evolution of the amplitude, then sample from ten thousand trajectories to obtain a distribution of amplitudes at certain times. This tells us how the trajectories can be expected to vary. Finally, we look at the distribution of times taken to jump between the metastable amplitudes.

Example System: Cesium

Cesium is an atom which is commonly used in atom trapping and cavity quantum electrodynamics. We use as an example an atomic transition in cesium which leads to the following parameters:

- **Transition wavelength**

$$\lambda = 852.4\text{nm}.$$

- **Spontaneous emission rate**

$$\gamma/2\pi = 2.6\text{MHz}.$$

- **Atomic mass**

$$m = 133\text{u}.$$

Using these parameters we apply the procedure outlined in the previous section. We plot two sample trajectories in Fig. 7.2. With the cesium parameters, the timescale of the graph is now in seconds. Only the order of magnitude here is significant because we have left out the effect of absorption and stimulated emission on the atomic motion, as discussed in Section 5.5. In Fig. 7.3 and Fig. 7.4 we plot the distribution of amplitudes $P_t(A)$. This is the probability for the atom to have an amplitude A at time t given the initial condition of $A = 0$ at $t = 0$.

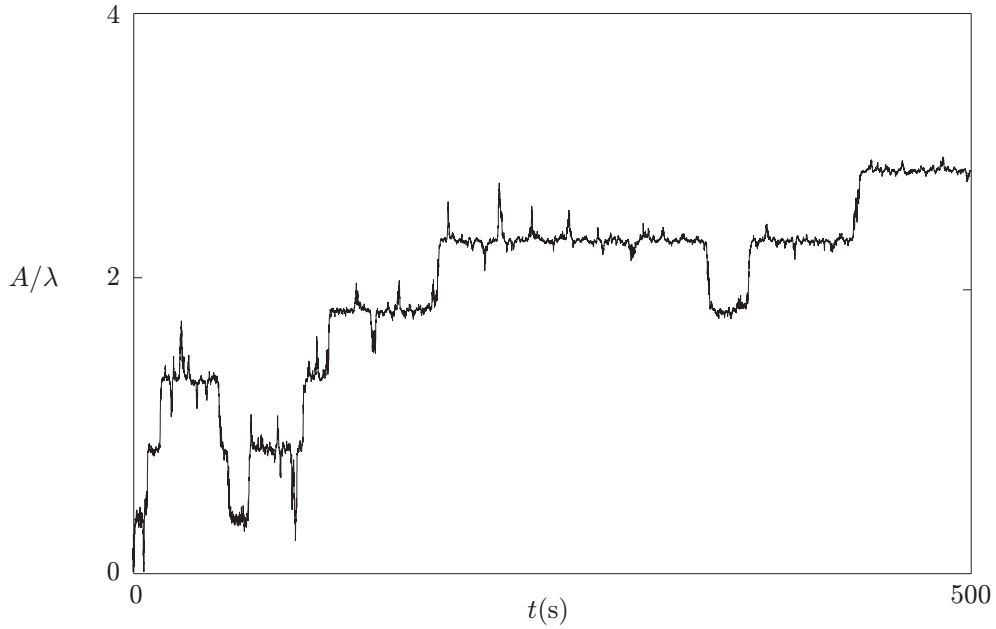

(a)

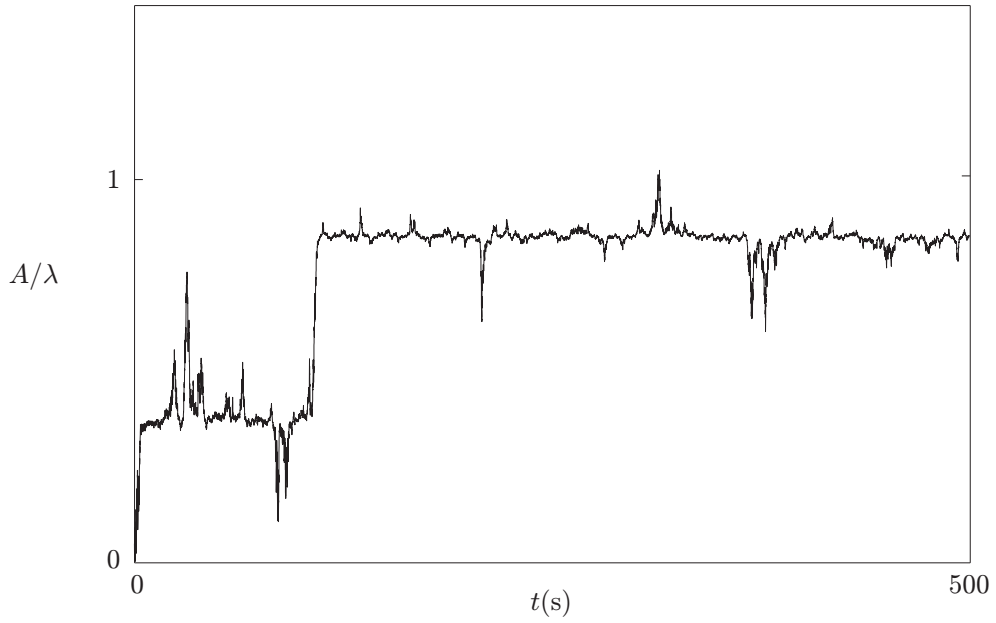

(b)

Fig. 7.2: Sample trajectories of the amplitude evolution using the diffusion model. (a) $\Omega_0 = \gamma$, $\omega_T = 2\gamma$. (b) $\Omega_0 = \gamma$, $\omega_T = 5\gamma$.

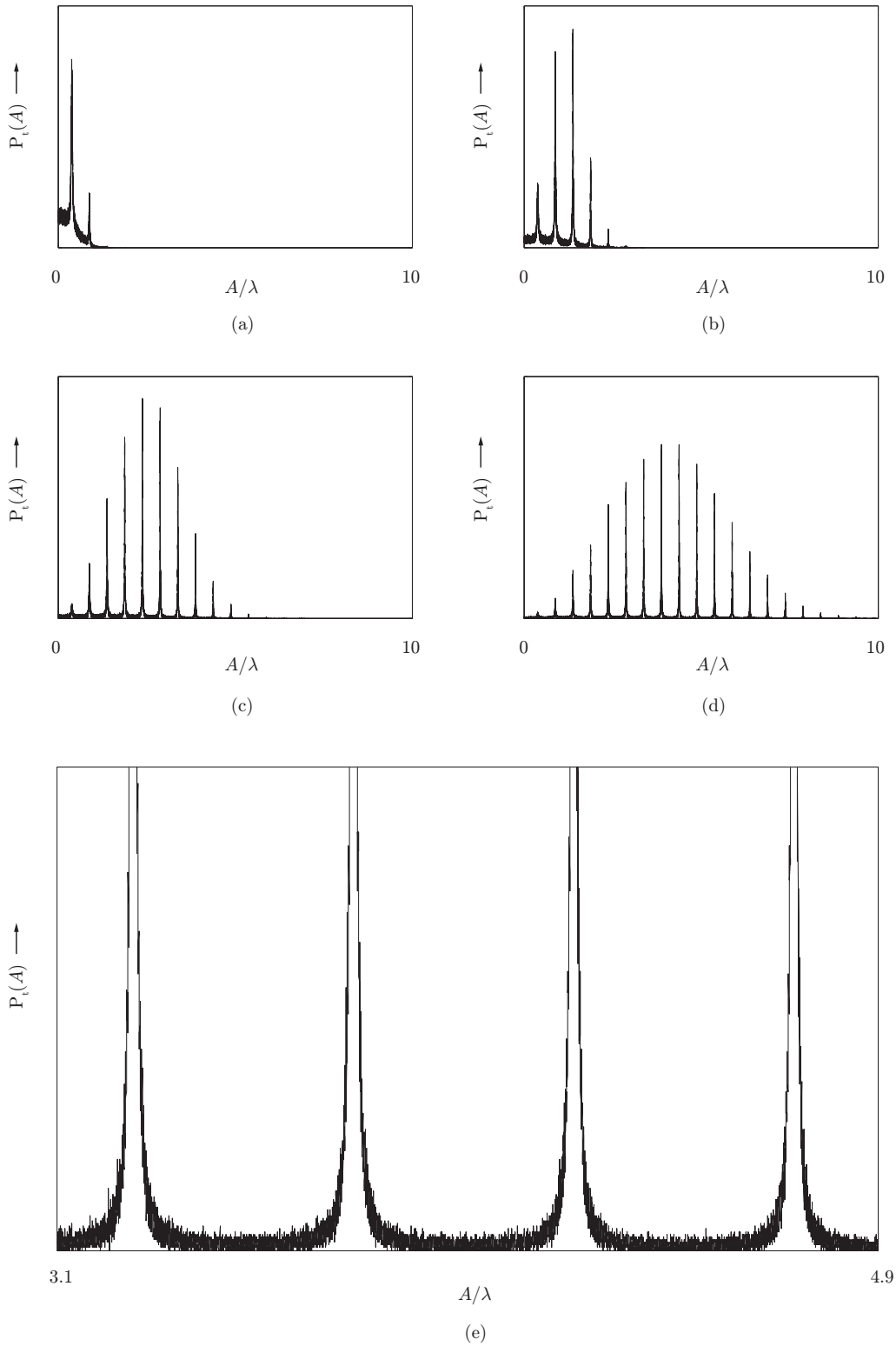

Fig. 7.3: Amplitude distribution for a heating cesium atom, with paramters $\Omega_0 = 5\gamma$ and $\omega_T = 5\gamma$. (a) $t = 4s$. (b) $t = 38s$. (c) $t = 385s$. (d) $t = 1923s$. (e) Zooming in at $t = 1923s$. To obtain this distribution we average 10^6 trajectories.

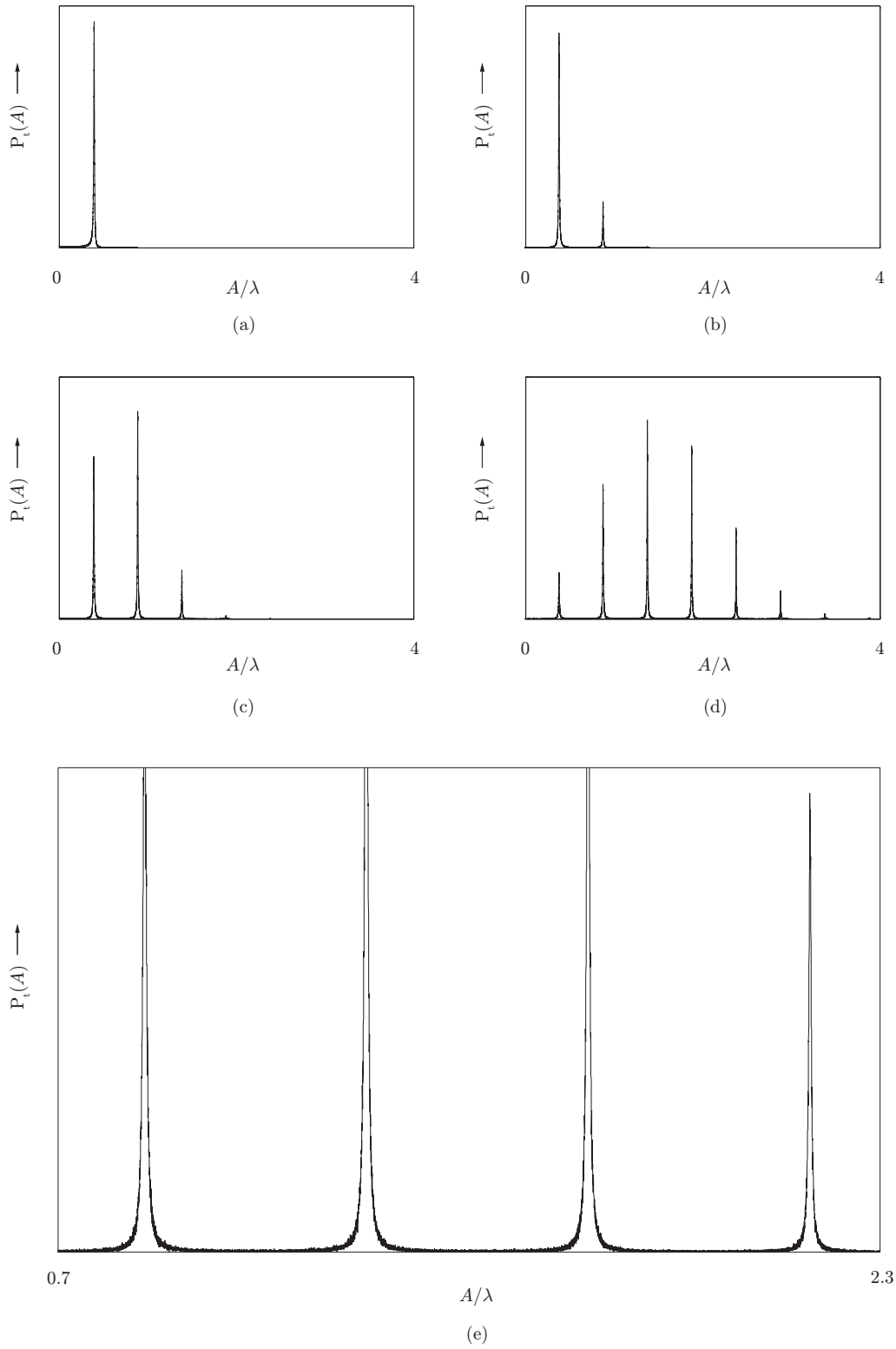

Fig. 7.4: Amplitude distribution for a heating cesium atom, with paramters $\Omega_0 = \gamma$ and $\omega_T = 10\gamma$. (a) $t = 38s$. (b) $t = 385s$. (c) $t = 1923s$. (d) $t = 19231s$. (e) Zooming in at $t = 19231s$. To obtain this distribution we average 10^6 trajectories.

Note: We cannot compare our new results to those of Chapter 5 using identical recoil velocities, as those used in Chapter 5 are far too large for our diffusion approximation to apply. However, we expect the differences in recoil velocity to only affect the timescale of the heating, not the qualitative features of the trajectories. Of course, comparing single trajectories does not tell you much; it is desirable to run many trajectories with each method and compare averages. For the quantum trajectory method this would take a lot of computing time, although the speed could certainly be increased using a more advanced numerical technique. This is an avenue for future research.

The parameters used in Fig. 7.4 result in a slower heating than we see in Fig. 7.3. We also see in both figures that the mean of the amplitude distribution will increase more slowly with time than the $\sqrt{t}$ dependence that is characteristic of a Wiener process. This is because, for larger amplitudes, the atom moves faster through a single wavelength of the standing wave; the Bloch vector has less time to move up the Bloch sphere before it changes direction, so the atom is on average less excited. Zooming in on the amplitude distribution we can see that, for the parameters used, the atom is much more likely to be found oscillating near a metastable amplitude. It is interesting that the atom spends a large proportion of its time around the ground state, where the spontaneous emission rate is greatly reduced. When it does move away from a metastable amplitude it quickly gets kicked around until it finds another. If one were to observe the atom oscillating in this system, it would appear to 'flash' each time it moved between metastable amplitudes, emitting a burst of photons. This hypothetical situation may not be realizable in an experiment, but it is a possible starting point in devising schemes to observe or utilise the strong amplitude dependence of the spontaneous emission rate. More will be said about experimental schemes in the next chapter.

In Fig. 7.5, the distribution of times taken to move from one metastable amplitude to an adjacent one is plotted. The tail of this distribution is well approximated by an exponential

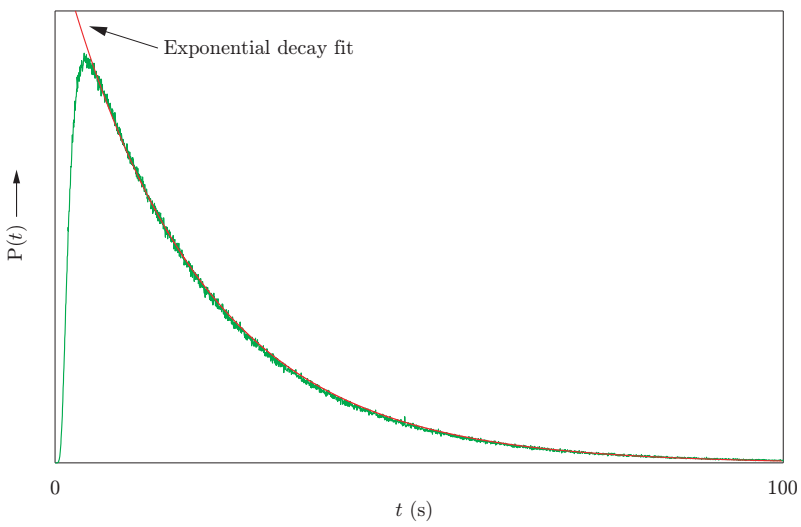

Fig. 7.5: Distribution of times taken for the amplitude to move from third peak ($A = 1.38$) to the fourth peak, with parameters $\Omega_0 = 5\gamma$ and $\omega_T = 5\gamma$. An exponential is fitted to the tail of the distribution. To obtain this distribution we sample from 10^6 trajectories.

decay, which we have fitted to the curve. This suggests that the heating could be further approximated by a process where the atom jumps between metastable amplitudes. Since the distribution of jump times is exponential, the atom would have a constant probability per unit time to make a transition, similar to a radioactive decay. Of course, the distribution is not exactly an exponential decay — there is zero probability for the atom to jump immediately to the next peak. This could be incorporated by adding intermediate states between the metastable amplitudes. This is not something we have investigated, but we point it out as a possible future direction.

Chapter 8

Conclusion

In this thesis we have developed a model of the random motion of a trapped atom driven at resonance by a standing-wave electromagnetic field. We have observed and quantified an interesting feature of this random motion: the dramatic amplitude dependence of the effective coupling between the atom and the field. As it heats up, the atom is much more likely to be found oscillating in the trap at certain discrete amplitudes. These 'metastable amplitudes' are separated by intervals of half the wavelength of the standing-wave.

8.1 A Summary of the Work

- In Chapter 5 we gave an explanation of the phenomenon: at the metastable amplitudes the time-averaged coupling is greatly reduced. Essentially, the 'imprint' left on the atom by the field as it moves between two nodes of the standing-wave is exactly undone as it moves between the next two. The atom stays down near its ground state, so it is much less likely to emit photons and get kicked around. We also discussed the approximations used and the regime in which our model is expected to hold.

- In Chapter 6 the effect was quantified further, using the mean time between spontaneous emissions. We developed an approximate analytical solution for this quantity (6.32) and showed that it had a strong dependence on the amplitude of oscillation. In the regime where it was expected to hold, this analytical solution was in very good agreement with the numerical solution that was also developed. Both numerical and analytical solutions were used to illustrate the parameter dependence of the phenomenon. The model was extended to include a detuning between the driving field and the atomic transition, and we showed numerically that the effect was still present, although it reduced, as the detuning increased. We also found that the effect remained when we moved the trap centre away from an antinode of the standing wave.

- In Chapter 7 we approximated the random motion by a diffusion process in order to characterise its statistical features. We showed how the individual trajectories could be expected to vary. Using parameters for a Cesium atom, we saw further evidence that these metastable amplitudes could appear in an experimental system.

8.2 Directions for Future Research

What we have presented in this thesis is a simplified model of a physical system. There is a domain in which it is expected to have some validity, but there are many complications and extensions to be investigated. We have discussed the domain of validity somewhat in Section 5.5, here we consider what can be extended. We would like to make extensions that are experimentally relevant, so we first discuss the experimental systems in which this effect might appear.

8.2.1 Experimental Considerations

We reiterate the criteria that are important for an experimental realization of our system:

- **An observable single atom**

  The random motion of one atom is expected to exhibit interesting behaviour. However, if the temperature or the scattered light is observed for a collection of atoms, the effect will average away as each atom will reach the metastable amplitudes at different times. It may of course be possible to see signatures of this effect in the statistical properties of the emitted light — that is something to be investigated further.

- **Effective one dimensional motion**

  The atom must be confined very tightly in all directions perpendicular to the propagation direction of the driving field. If this constraint is removed the metastable amplitudes may well remain in some form, but our simple model will not apply.

- **On resonance excitation**

  The driving field must be tuned as close as possible to the resonant frequency of the atomic transition for the strongest effect to be seen.

- **Low driving field intensity**

  The maximum rabi frequency Ω_0 (set by the average intensity of the driving field) should be similar to, or smaller than, the spontaneous emission parameter γ.

- **High trap frequency**

  The frequency ω_T of the trap in the the direction of propagation of the driving field should be larger than the the spontaneous emission parameter γ. Taking cesium as an example (with $\gamma/2\pi = 2.6$MHz) a trap frequency of around 5MHz or higher is preferable.

- **High temperature**

  With a high trap frequency, to get out to amplitudes of several wavelengths (and also for the motion to be described classically) the atom must be 'hot' so that it is high up in the energy levels of the trap. Again for cesium with a trap frequency of 5MHz, the temperature should be of the order of a few Kelvin.

Promising candidates for an experimental observation of the metastable amplitudes are the ion traps (Paul traps) that have been developed extensively over the last few decades. An investigation of how these ion trap systems should be configured to observe this effect is a possible future direction.

8.2.2 Other Extensions

An interesting direction for future research is to treat the motion of the atom in the trap quantum mechanically. In our model we treat the motion classically and add spontaneous emission recoil artificially in our Monte Carlo simulations; we also ignore completely the effect on the motion of the atom's coherent interaction with the driving field. We could instead extend our Hilbert space to include the centre-of-mass motion of the atom as well as its internal state. All photon absorptions and emissions would then affect the motion. It is also of interest to see how things change when the atom is cooled to the lower energy levels of the trap, since this regime is accesible experimentally in the ion traps we have mentioned. A quantised treatment of the motion is essential in this regime.

Another thing to be investigated is how the metastable amplitudes change as the atom is allowed to move in all three dimensions. This is not too difficult to do, as the mean waiting time can still be calculated numerically. However, the system becomes more complex and a thorough characterisation of the parameter space is a considerable task.

Appendix A

Bessel Functions

We review some basic properties of Bessel functions. Bessel functions of are defined as the solutions to the differential equation

$$x^2 \frac{d^2y}{dx^2} + x\frac{dy}{dx} + \left(x^2 - n^2\right) y = 0, \tag{A.1}$$

which is known as Bessel's differential equation. The solutions that are nonsingular at the origin are called Bessel functions of the first kind, which we denote by $J_n(x)$. These functions are normalised so that

$$\int_0^\infty J_n(x)\, dx = 1. \tag{A.2}$$

The parameter n is called the *order* and can be any real number, although the most interesting case is when n is an integer. For integer order, Bessel functions of the first kind can be defined via the generating function

$$e^{(x/2)(t-1/t)} = \sum_{n=-\infty}^{\infty} J_n(x) t^n, \tag{A.3}$$

and from this definition it follows that

$$\sum_{n=-\infty}^{\infty} J_n(x) = 1. \tag{A.4}$$

A useful property of these functions is

$$J_{-n}(x) = (-1)^n J_n(x), \tag{A.5}$$

which can be shown via a series solution to (A.1) and holds for integer n only. Another property that holds for integer n is the Jacobi-Anger identity

$$e^{ix\cos\theta} = \sum_{n=-\infty}^{\infty} i^n J_n(x) e^{in\theta}. \tag{A.6}$$

From this identity it follows that

$$e^{ix\sin\theta} = \sum_{n=-\infty}^{\infty} J_n(x) e^{in\theta}. \tag{A.7}$$

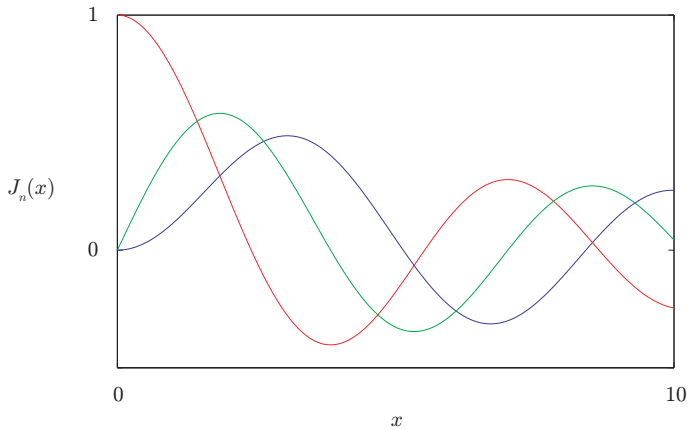

Fig. A.1: Bessel functions of the first kind for $n = 0$ (red line), $n = 1$ (green line), and $n = 2$ (blue line).

In the limit where $0 < x << \sqrt{n+1}$, the Bessel functions of postive order approach

$$J_n(x) \longrightarrow \frac{1}{\Gamma(n+1)} \left(\frac{x}{2}\right)^n, \tag{A.8}$$

where Γ denotes the gamma function. In the opposite limit where $x >> \left|n^2 - 1/4\right|$ they become

$$J_n(x) \longrightarrow \sqrt{\frac{2}{\pi x}} \cos\left(x - \frac{n\pi}{2} - \frac{\pi}{4}\right), \tag{A.9}$$

so we can see that for large x the zeros of $J_n(x)$ are separated by intervals of 2π. The first three Bessel functions of integer order are illustrated in Fig. A.1. The basic shape is well described by the large x limit: a sinusoidal oscillation with an amplitude that decays with a $x^{-\frac{1}{2}}$ dependence. Bessel functions have many other useful properties which we do not state here as they aren't used in this thesis. A more comprehensive summary can be found in Abramowitz and Stegun [24].

Bibliography

[1] W. Neuhauser, M. Hohenstatt, and P. E. Toschek: Phys. Rev. A **22**, 1137 (1980)

[2] Wolfgang Paul: Rev. Mod. Phys. **62**, 531 (1990)

[3] T. W. Hänsch and A. L. Schawlow: Opt. Commun. **13**, 68 (1975)

[4] D. J. Wineland and H. G. Dehmelt: Bull. Am. Phys. Soc. **20**, 637 (1975)

[5] F. Diedrich, J. C. Bergquist, W. M. Itano, and D. J. Wineland: Phys. Rev. Lett. **62**, 403 (1989)

[6] D. Leibfried, E. Knill, S. Seidelin, J. Britton, R. B. Blakestad, J. Chiaverini, D. B. Hume, W. M. Itano, J. D. Jost, C. Langer, R. Ozeri, R. Reichle, and D. J. Wineland: Nature **438**, 639 (2005)

[7] H. Häffner, W. Hänsel, C. F. Roos, J. Benhelm, D. Chek-al-kar, M. Chwalla, T. Körber, U. D. Rapol, M. Riebe, P. O. Schmidt, C. Becher, O. Ghne, W. Dür, and R. Blatt: Nature **438**, 643 (2005)

[8] E. L. Raab, M. Prentiss, A. Cable, S. Chu, and D. E. Pritchard: Phys. Rev. Lett. **59**, 2631 (1987)

[9] J. I. Cirac, P. Zoller, H. J. Kimble, and H. Mabuchi: Phys. Rev. Lett. **78**, 3221 (1997)

[10] J. McKeever, J. R. Buck, A. D. Boozer, A. Kuzmich, H.-C. Nägerl, D. M. Stamper-Kurn, and H. J. Kimble: Phys. Rev. Lett. **90**, 133602 (2003)

[11] J. McKeever, A. Boca, A. D. Boozer, J. R. Buck, and H. J. Kimble: Nature **425**, 268 (2003)

[12] C. J. Hood, T. W. Lynn, A. C. Doherty, A. S. Parkins, and H. J. Kimble: Science **287**, 1447 (2000)

[13] G. Rempe, R. J. Thompson, R. J. Brecha, W. D. Lee, and H. J. Kimble: Phys. Rev. Lett. **67**, 1727 (1991)

[14] J. J. Sakurai: *Modern Quantum Mechanics, Revised Edition* (Addison-Wesley, 1994)

[15] E. Merzbacher: *Quantum Mechanics, Third Edition* (Wiley, 1998)

[16] F. Bloch: Phys. Rev. **70**, 460 (1946)

[17] H. J. Carmichael: *Statistical Methods in Quantum Optics 1: Master Equations and Fokker-Planck Equations* (Springer-Verlag, 1999)

[18] H. Haken: *Handbuch der Physik*, Vol. XXV/2c, ed. by L. Genzel (Springer-Verlag, 1970)

[19] H. J. Carmichael: *An Open Systems Approach to Quantum Optics* (Springer-Verlag, 1993)

[20] H. J. Carmichael and D. F. Walls: J. Phys. B **9**, L43 (1976)

[21] H. J. Kimble, M. Dagenais, and L. Mandel: Phys. Rev. Lett. **39**, 691 (1977)

[22] H. J. Carmichael, S. Singh, R. Vyas, and P. R. Rice: Phys. Rev. A **39**, 1200 (1989)

[23] C. W. Gardiner: *Handbook of Stochastic Methods for Physics, Chemistry and the Natural Sciences, Second Edition* (Springer-Verlag, 1985)

[24] M. Abramowitz and I. A. Stegun: *Handbook of Mathematical Functions* (Dover, 1970)